Geochemical Characterization of Organic Rich Black Rocks of the Niutitang Formation to Reconstruct the Paleoenvironmental Settings during Early Cambrian Period from Xiangxi Area, Western Hunan, China

Rizwan Sarwar Awan ⓞ *[1, 2], **Chenglin Liu** ⓞ *[1, 2], **Ashar Khan**[3], **Khawaja Hasnain Iltaf**[1, 2],
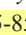
Qibiao Zang[1, 2], **Yuping Wu**[1, 2], **Sajjad Ali**[1, 2], **Muhammad Amar Gul**[4]

1. *College of Geosciences, China University of Petroleum, Beijing 102249, China*
2. *State Key Laboratory of Petroleum Resource and Prospecting, China University of Petroleum, Beijing 102249, China*
3. *Water and Power Development Authority, Lahore 54000, Pakistan*
4. *School of Earth and Space Sciences, University of Science and Technology, Hefei 230026, China*
ⓞRizwan Sarwar Awan: https://orcid.org/0000-0003-4035-8579; ⓞChenglin Liu: https://orcid.org/0000-0001-9075-5228

ABSTRACT: The Niutitang Formation in the South China Block might be a source of hydrocarbon as it contains an enormous quantity of organic matter. Black rock of the Early Cambrian Niutitang Formation is widely distributed in the Yangtze region, but detailed geochemical understanding of it is still emerging. This research discusses the detailed geochemical characteristics of the Niutitang Formation to reconstruct the paleoenvironmental conditions, employing total organic carbon (TOC) content, major, trace, and rare earth element data. For this purpose, black rock specimens of the Niutitang Formation from two outcrop sections were utilized for geochemical characterization, and the results compared with another eight sections from the South China Block. The average total organic carbon in these sediments is significantly higher (5.80 wt.%). In the platform region, lower quantities of TOC indicate a poor potential to produce hydrocarbons. At the same time, significantly higher TOC is observed in the deep shelf and slope sediments, indicating a significant potential to produce hydrocarbons. The average Ce, Eu and Y anomalies from both Longbizui and Sancha sections studied are 0.74, 0.86, 1.77, 1.07, and 1.19, 1.30, respectively. The chemical index of alteration (CAI) throughout the Yangtze block is higher (averaging 71.32) than that of Post Archean Australian Shale (PAAS 69), indicating a moderately weathered source of the Niutitang Formation relative to PAAS. As the sediments are moderately weathered, this suggests these rocks might have been derived from felsic rocks, mainly granite-granodiorite. The normalization of REEs in the black rocks reveals a reduction of light REEs with increase in heavy REEs enrichment. Similarly, a positive Eu anomaly, negative Ce anomaly, and a moderate Y/Ho (34.61) are clues to a hybrid depositional mechanism associated with hydrothermal action and terrigenous input. These anomalies are also evidence of upwelling in the paleo-ocean and mixing of organic matter, which created anoxic bottom water during the deposition of the Niutitang Formation in the basin and upper oxic water conditions before deposition. The main controlling factors for the distribution of rare earth elements in these black rocks of the Niutitang Formation are pH, terrigenous input, source rock composition, tectonism, an upwelling mechanism, and hydrothermal activity.
KEY WORDS: anomaly, paleo-ocean, paleoenvironment, chemical index, alteration, weathering, metasomatism, sediments.

*Corresponding authors: rsageoche@gmail.com;
liucl@cup.edu.cn

0 INTRODUCTION

Black rock sediments or black shales are widely distributed around the globe (Fig. 1a). The Early Cambrian was a unique period of geological time due to a dramatic increase in diversity in the abundance of fossils, also known as the Cambrian Explosion (Pi et al., 2013; Amthor et al., 2003). Variations in the ambient conditions provide a feasible rationale for evolutionary heterogeneity; but remains a subject of discus-

sion. Early Cambrian marine sedimentary rocks are widely distributed all over South China (Fig. 1c). The Niutitang Formation comprises various types of black sediments, e. g., shale, black shale, siliceous shale, sandstone, silty shale, mudstone, and silty mudstone, that have been described as the black rock series (Awan et al., 2020). These rocks provide a new type of mineral resource in China due to their enrichment of some valuable elements, e.g., molybdenum, vanadium, and uranium, but so far there has not been substantial exploitation of these elements. Three aspects of the Cambrian Explosion are displayed in the Niutitang Formation: (i) the existence of ancient remains of arthropods in black shale; (ii) the presence of ancient remains of tiny shells in phosphorites; (iii) the presence of metazoans and trilobites in green/grey shales (Pi et al., 2013; Steiner et al., 2007; Weber et al., 2007). Shen et al. (2000) and Shields and Stille (2001) proposed that environmental conditions in South China were transformed due to bottom anoxic settings preceding the first phase of the Cambrian Explosion. Weathering (especially chemical weathering) in a rock is a significant geological action that transforms the earth's surface and regulates the elemental geochemical cycle, and thus controls global climatic conditions.

REEs or lanthanides are a series of heavy elements usually with similar chemical characteristics. They comprise 15 elements from La to Lu, with atomic numbers from 57 for La to 71 for Lu. REEs are extensively used in research to explore the chemical evolution (CE) of the continental crust (Singh, 2009; Yang et al., 2002; Singh and Rajamani, 2001). They can also be used to determine chemical or biochemical weathering in the drainage areas of basins, the source provenance of sediments, paleoenvironmental variations in the oceans, and tectonic settings (Jiang et al., 2019; Munksgaard et al., 2003; Rudnick and Gao, 2003; McLennan, 2001). During weathering processes, rare earth elements may be mobile throughout a profile, mainly during the initial phase of weathering. REE distributions in different rock profiles are variable under low pH conditions. As pH rises to 7 or beyond in an alkali pH phase, REEs are precipitated or adsorbed on the surfaces of hydroxides or clays (Singh and Rajamani, 2001; Sharma and Rajamani, 2000a). Many researchers have observed that REEs could then become redistributed in a discontinuous rock profile. In contrast, cumulative losses or gains of a particular rare earth element that does not escape from the network may not occur (Sharma and Rajamani, 2000a, b). Generally, REEs are highly concentrated in rocks containing fine particles if their host minerals containing primary and secondary REEs have fine particle sizes.

The series of rare earth elements with a higher atomic number are designated as heavy rare earth elements (HREEs). In contrast, the lower atomic number elements are known as light rare earth elements (LREEs). Also, the middle rare earth elements (MREEs) have been designated as the elements that range from samarium to holmium (Dubinin, 2004). Due to the short residence span of 102–103 years of REEs in ocean water relative to the ocean's mixing period of approximately 1 600 years, these elements have been used to reveal ancient oceanic process (Grandjean et al., 1988). Generally, the light rare earth elements (La-Sm) are mainly associated with trace minerals such as apatite, while the HREEs (Gd-Lu) are particularly relat-

ed to zircon. The REEs are naturally enriched at deeper earth horizons as REEs are adsorbed or precipitated on oxyhydrates of clays, whereas they are depleted in near-surface horizons. Some REEs, e.g., La, Tb, Ce, Dy, Lu, and Yb, have a strong tendency to accompany organic matter (OM) relative to Eu and Sm (Zhuang et al., 1998) Previous research on black rocks have revealed enrichments of sapropelic OM, which originated from marine plankton. Also, the degree of pyritization suggests euxinic bottom water settings (Awan et al., 2020).

In this study we aim to: (1) present fractionation and concentration patterns of the rare earth elements in black sediments of the Niutitang Formation in the Yangtze Block; (2) illustrate the factors influencing REE concentration; and (3) provide a theoretical framework to reveal the metallogenic settings, genesis, and redox environment of black rocks using various geochemical characteristics.

1 GEOLOGY AND TECTONICS

Multiple events caused fragmentation of Rodinia during Neoproterozoic time and the final phase of splitting and drifting took place during the period 750–690 Ma (Liu et al., 2015). In North China, the Cathasian and Yangtze blocks were separated during the Ediacaran–Early Cambrian periods. A deep rifted marine basin had arisen surrounding of the periphery of the Yangtze Block (Cai and Liu, 1996). At that time, the Yangtze Block was situated in the equatorial zone close to the S-W of the Australian Plate (Fig. 1) (Liu and Xu, 1994). Due to continuing tectonic activity in the Ediacaran to the Early Cambrian period, paleo-settings of the present research area were transformed from a shallow to a deep marine shelf or slope environment, from carbonates to argillaceous rocks (Liu et al., 2015; Zhu et al., 2003). Recent studies reveal that the Early Cambrian was marked by a maximum flooding span in the Yangtze region, which ended in an anoxic ocean event (OAE) of early Tommotian age, and developed suboxic to anoxic bottom water settings on a massive scale (Liu et al., 2015; Jiang et al., 2011; Li et al., 2010; Wang et al., 2007). The Niutitang Formation and its stratigraphic equivalents are comprised of black shale deposits on the Yangtze Block, especially on the slope. It is generally suggested that phosphorites at the base of the Cambrian indicate strong upwelling (Wille et al., 2008; Clark et al., 2004). Some black shales are related to metallic ores (Fe-Ni-Mo) which were deposited during hydrothermal episodes in the Cambrian period (Orberger et al., 2007; Steiner et al., 2001). Another indicator of Cambrian hydrothermal activity is higher values of a Eu anomaly in phosphate nodules within the shales (Zhu et al., 2014). Various metallic ratios (Co-Cu-Ni-PGE) suggest ultramafic and mafic sources for these rocks (Han et al., 2015). A few studies indicate a primary source for these metallic ores in these black sediments due to seawater in a silled basin leading to long periods of stratigraphic condensation (Och et al., 2013; Lehmann et al., 2007).

In the eastern Yunnan region, the geologic age of the lower part of the Niutitang Formation is 540–536 Ma based on U-Pb dating. The Guizhou area shows relatively younger ages suggesting territorial diachroneity, for instance, 522.7 ± 4.9 (Wang et al., 2012) and 532.3 ± 0.7 (Jiang et al., 2009). The central part of the black Niutitang Formation is dated to 521.0 ± 5.0 us-
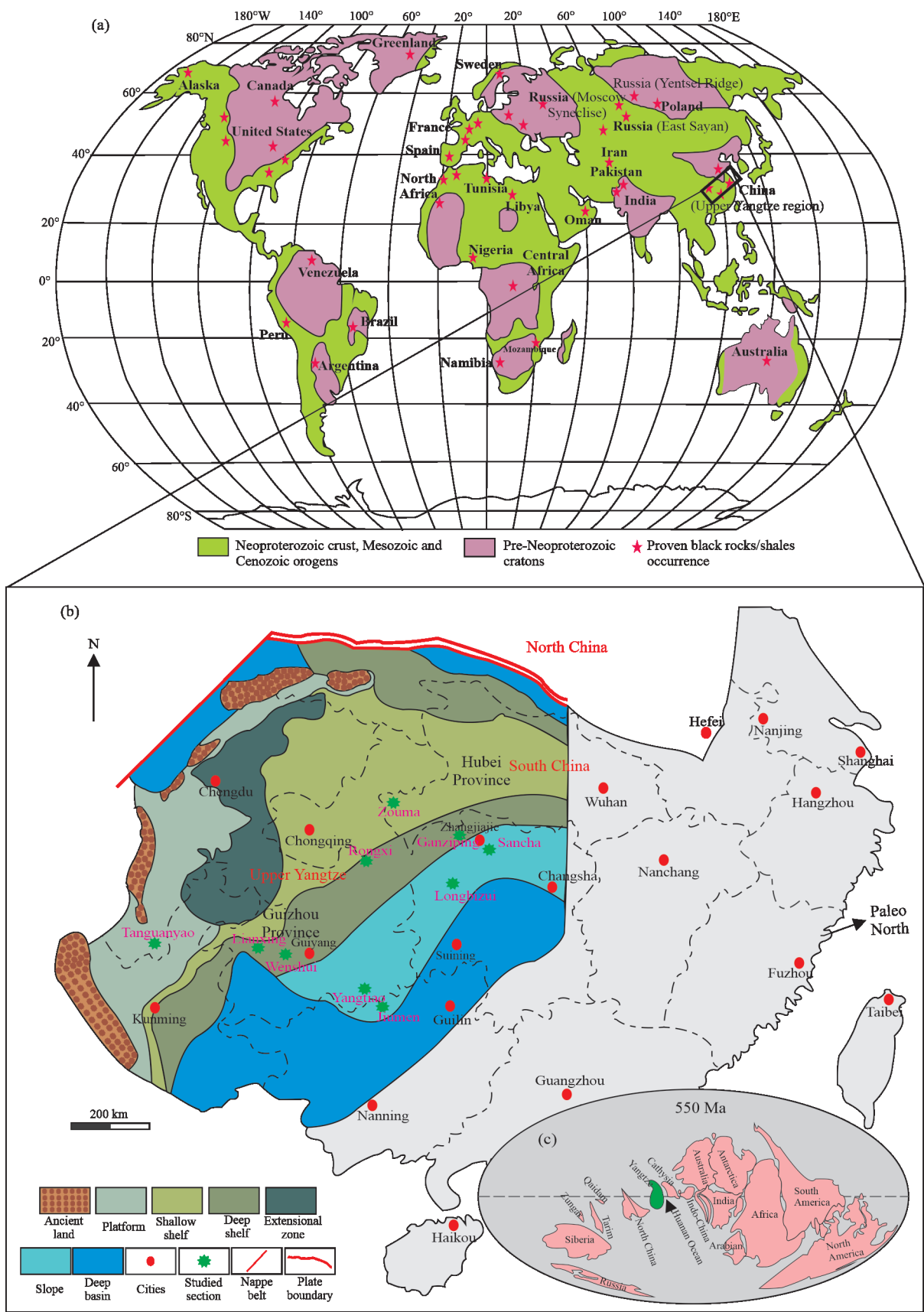
Figure 1. (a) Sketch map showing the global distribution of black rock/shales (Awan et al., 2020) and the location of Yangtze Block in South China; (b) paleogeographic map of the Upper Yangtze region, deciphering the different lithofacies (modified after Zhang et al., 2018; Luo, 2014; Steiner et al., 2001); (c) global paleogeography during the Early Cambrian period (modified after Liu et al., 2015).

ing Re-Os dating (Xu et al., 2011). The deposition age of the Niutitang Formation in the Guizhou area shows relatively younger ages suggesting territorial diachroneity, for instance, 522.7 ± 4.9 (Wang et al., 2012) and 532.3 ± 0.7 (Jiang et al., 2009). The central part of the black Niutitang Formation is dated to 521.0 ± 5.0 using Re-Os (Xu et al., 2011). The deposition age of the Niutitang Formation based on recent research is 3–12 Ma, which started at 532–523 and stopped at approximately 520 Ma from the bottom to the top. The average thickness of Niutitang Formation based on recent research is 3–12 Ma, which began at 532–523 and stopped at approximately 520 Ma. The average thickness of Niutitang Formation in the present research area is 76 m, which shows that the rate of deposition was about 6–7 up to nearly 25 m/Ma (Xu et al., 2012).

2   MATERIALS AND METHODOLOGY

Fresh black rock specimens of the Niutitang Formation were selected for quantitative examination of REEs from two outcrop sections at Longbizui and Sancha and compared with published data from eight other outcrop sections. Samples were collected at the outcrop section after digging at the sample point up to 0.6 m depth. Niutitang Formation in South China mainly comprises various types of black sediments, e. g., shale, carbonaceous shale, siliceous shale, sandstone, silty shale, mudstone, and silty mudstone, as shown in the supplementary materials (Fig. S1). A LECO CS230 instrument was used to determine the quantity of total organic carbon content (TOC). The crushed and ground samples were initially passed through a sieve (<200). After that, for 24 h, the samples were cleaned with diluted hydrochloric acid (HCL 5%) at 60 °C to eliminate inorganic carbon and carbonates and then purified water was used to eradicate the added HCl. Samples were then put into an oven for 24 h at 50 °C. At a higher temperature of 900 °C, the specimens were combusted utilizing an oxygen-rich carrier gas. The remaining organic C was entirely oxidized to CO_2, and the bulk volume of produced CO_2 was utilized to compute TOC. X-ray fluorescence spectrometry was used to determine the major elements using the AB1041/AL104 Axiosmaxat the State Key Laboratory of Petroleum Resources and Prospecting, China University of Petroleum Beijing, China (CUPB). The powdered specimen was oxidized for an hour at 920 °C to eradicate the organic matter. Finally, the 500 mg specimen was intermixed to 4 000 mg of $Li_2B_4O_7$ and incorporated in a disk of glass at 1 150 °C. These experiments were performed using standard criteria with relative humidity and temperature of 31% and 23 °C.

The concentration of trace and rare earth elements was determined by Nex ION300D plasma mass spectroscopy using the Peoples Republic of China National Standard GB/T 14506.

30—2010 at the Laboratory of Hebei Institute of Regional Geology & Mineral Resources, with an analytical precision of ±5%. Powdered samples were placed in a 700 °C furnace for 3 h to remove organic matter, and specimens were dissolved into solution using acids. The standard method is appropriate under temperature and relative humidity of 21 °C and 32%, respectively and inaccuracies in this method are below 10%. Elemental concentrations can be expressed as enrichment factors (EF) based on the standardization of aluminum (Al) or titanium (Ti) (Brumsack, 1989). For example, the EF of element X can be expressed as $EFX = (X/Al)_{sample}/(X/Al)_{UCC}$, in which the ratio in the denominator is based on upper continental crust (UCC) values (Tribovillard et al., 2006). A calculated EF > 1 means the shale is enriched with respect to a given element, whereas an EF < 1 means the shale is depleted in a given element.

3   RESULTS
3.1   Total Organic Carbon (TOC)

In this research, we collected 27 outcrop samples from two Longbizui (LA) and Sancha (CR) sections to determine the TOC. The amount of TOC from the Longbizui Section ranges from 0.65 wt.% to 8.16 wt.% with a mean value of 3.34 wt.%. In contrast, a significantly higher TOC between 5.47 wt.% and 9.96 wt.% with an average value of 8.09 wt.% content was noticed in the samples from the Sancha Section (Table 1).

3.2   Elemental Geochemistry

The concentrations of some major oxides and their calculated parameters are tabulated in Table 2. The oxides of major elements show a higher concentration of SiO_2 from the Sancha and the Longbizui sections with a mean value of 65.61 wt.% and 69.50 wt.%, respectively. Other oxides with concentrations of 1.0 wt.%–10 wt.% are Al_2O_3, Fe_2O_3, CaO, and K_2O. The average values of MgO and P_2O_5 from the Sancha Section are greater than 1.0 wt.%, while the Longbizui Section contains lower values. The remaining major oxides, TiO_2, MnO, and Na_2O, have lower concentrations (<1.0 wt.%) in these sediments. Trace elemental compositions are diverse. Barium and vanadium have a substantially higher value in the Niutitang Formation from both studied Longbizui and Sancha sections with an average value of 15 444 ppm and 1 419 ppm, 641.7 ppm and 653.69 ppm, respectively. A few trace elements such as Zr, Ni, and Cr, have a moderately higher concentration from Longbizui and Sancha sections with typical values of 80.98 ppm and 67.69 ppm, 70.49 ppm and 119.84 ppm, 160.95 ppm and 60.78 ppm, respectively. The mean concentrations of Mo and U from the Longbizui and Sancha sections are 37.54 ppm and 140.38 ppm, 24.62 ppm and 52.39 ppm, respectively. Some trace metals such as Co and Th

Table 1   Total organic carbon content (wt.%) in the black rocks of Niutitang Formation from different sections of Yangtze Block

Longbizui	Sancha	Rongxi (Gao et al., 2018)	Ganziping (Pan et al., 2004)	Lianxing (Jia et al., 2018)	Wenshui (Jia et al., 2018)	Yangtiao (Jia et al., 2018)	Jiumen (Jia et al., 2018)	Tanguanyao (Zhou et al., 2017)	Zouma (Zhou et al., 2017)
(0.65–8.16)	(5.37–9.96)	(0.5–18.2)	(0.27–12.31)	(0.99–3.85)	(2.77–3.51)	(1.41–7.25)	(2.13–6.45)	(0.15–0.63)	(0.21–3.23)
3.34(13)	8.09(14)	8.65(17)	7.43(19)	2.74(4)	3.11(5)	3.65(5)	4.7(4)	0.30(9)	1.50(14)

$\frac{Range}{Mean\,(sample\,amount)}$, the same as in the following tables.

Table 2 Major (wt.%) and trace elements (ppm) concentrations and some parameters

Section	SiO$_2$	Al$_2$O$_3$	Fe$_2$O$_3$	MgO	CaO	Na$_2$O	K$_2$O	MnO	TiO$_2$	P$_2$O$_5$	CIW
Longbizui	46.06–92.22 / 69.50(13)	0.21–16.13 / 9.24(13)	0.16–6.38 / 2.9(13)	0.20–1.77 / 0.88(13)	0.14–8.24 / 1.28(13)	0.12–2.11 / 0.93(13)	0.04–3.45 / 2.10(13)	0.004–0.027 / 0.009(13)	0.09–0.74 / 0.57(13)	0.02–0.75 / 0.18(13)	82.68–94.56 / 90.38(13)
Sancha	24.27–78.76 / 65.61(14)	3.35–9.46 / 6.84(14)	0.74–5.45 / 3.65(14)	0.47–4.33 / 1.20(14)	0.08–30.88 / 3.30(14)	0.08–0.563 / 0.33(14)	1.04–3.76 / 2.51(14)	0.004–0.042 / 0.016(14)	0.12–0.44 / 0.30(14)	0.035–22.88 / 1.75(14)	85.34–98.61 / 94.49(14)

Section	ICV	SiO$_2$/Al$_2$O$_3$	MnO/TiO$_2$	Al/Na	K$_2$O/Al$_2$O$_3$	V	Cr	Ni	Co	Mo	Ba	Zr
Longbizui	0.55–1.96 / 0.93(13)	4.21–19.70 / 8.09(13)	0.09–0.74 / 0.57(13)	6.21–16.63 / 10.52(13)	0.17–0.26 / 0.23(13)	74.6–3 398 / 641.7(13)	25.5–1 001 / 160.95(13)	9.36–265 / 70.49(13)	1.66–25.8 / 7.15(13)	6.2–92.3 / 37.54(13)	1 423–21 390 / 15 444(13)	6.87–158 / 80.98(13)
Sancha	0.65–1.97 / 1.24(14)	5.98–12.64 / 9.62(13)	0.12–0.44 / 0.30(13)	14.12–44.40 / 19.64(14)	0.33–0.39 / 0.36(14)	228–948 / 653.69(13)	46.4–107 / 60.78(13)	42.2–212 / 119.84(13)	0.89–23.3 / 16.78(13)	65.9–330 / 140.38(13)	727–5 340 / 1 419(14)	50.4–99.9 / 67.69(14)

Section	Th	U	EF$_{Sb}$	EF$_{Rb}$	EF$_{cs}$	EF$_{Zr}$	EF$_{Ta}$	EF$_{Nb}$	EF$_{Hf}$	EF$_U$	EF$_V$
Longbizui	0.54–15.1 / 8.09(13)	4.45–62.7 / 24.62(13)	1.5–364.0 / 83.93(13)	0.47–0.73 / 0.63(13)	0.55–4.18 / 1.23(13)	0.54–1.41 / 0.53(13)	0.44–1.52 / 0.68(13)	0.54–1.27 / 0.76(13)	0.25–1.30 / 0.51(13)	2.37–238.1 / 52.12(13)	1.8–11.24 / 4.94(13)
Sancha	3.76–6.75 / 5.78(14)	27.9–78.1 / 52.39(14)	8.76–48.01 / 24.10(14)	0.65–0.86 / 0.71(14)	1.23–2.67 / 1.42(14)	0.32–0.47 / 0.40(14)	0.43–0.60 / 0.51(14)	0.49–0.72 / 0.63(14)	0.33–0.40 / 0.36(14)	37.57–186.9 / 105.69(14)	1.04–38.85 / 14.68(14)

have lower values from both Longbizui and Sancha sections, with a median value of 7.15 ppm and 16.78 ppm, 8.09 ppm, 5.78 ppm (Table 2). Total rare earth elements (ΣREE) from the Longbizui Section range of 58.66 ppm to 395.68 ppm, with an average value of 174.87 ppm, while the values of the total rare earth elements (ΣREE) from the Sancha Section vary from 102.51 ppm to 423.09 ppm with a mean value of 156.02 ppm (Table 3). The light rare earth elements and the heavy rare earth elements are La, Pr, Ce, Sm, Eu, Nd; and Gd, Ho, Tm, Dy, Yb, Tb, and Lu, respectively (Taylor and McLennan, 1985). The mean value of light rare earth elements (LREEs) from the Longbizui part (126.76 ppm) is higher than the Sancha Section (101.28 ppm). Only one sample from the Longbizui Section contains LREEs values lower than 50 ppm (around 40.05 ppm). However, most of the samples comprise higher content of LREEs (over 100 ppm) with a higher value of 231.32 ppm at the lower part of the Longbizui Section. Similarly, the average amount of heavy rare earth elements (HREEs) from the Sancha Section (13.59 ppm) is slightly lower than the Longbizui Section (14.87 ppm). In the same way, the ratio of light rare earth elements to heavy rare earth elements (LREE/HREE) from the Longbizui and Sancha sections average 10.02 ppm and 8.311 ppm, respectively. The average quantity of yttrium from the Longbizui and Sancha sections is 39.32 ppm and 41.32 ppm, respectively, lower than the average values of Rongxi and Jiumen. On the other hand, the Y/Ho ratios from the Longbizui and Sancha sections are 34.54 ppm and 36.69 ppm, respectively (Table 3). Different REEs anomalies were calculated via the following formulae after Jia et al. (2018); Shields and Stille (2001); Steiner et al. (2001).

$$Eu/Eu^* = \frac{Eu_N}{\sqrt{Sm_N \times Gd_N}}$$

$$Pr/Pr^* = \frac{2Pr_N}{Ce_N + Nd_N}$$

$$Ce/Ce^* = \frac{3Ce_N}{2La_N + Nd_N}$$

$$Y/Y^* = \frac{2Y_N}{Dy_N + Ho_N}$$

$$\delta U = \left(\frac{U}{\frac{1}{2}\left(U + \frac{Th}{3}\right)} \right)$$

These specimens for REEs were computed by normalized Post Archean Australian Shale (PAAS), where the standard constraints are marked by the sub-index N (McLennan, 2001; Taylor and McLennan, 1985). The value of the cerium anomaly from the Longbizui Section is 0.74 ppm, whereas the Sancha Section is 0.86 ppm. The Eu anomalies in these dark sediments from the Longbizui and Sancha sections are 1.77 and 1.07, respectively. Additionally, the Pr anomaly at the Longbizui and Sancha sections varies of 0.99 ppm–1.18 ppm and 0.90 ppm–1.12 ppm, respectively (Table 3).

Table 3 Rare earth elements (REEs) (ppm) in the black rocks of Niutiang Formation from different sections of Yangtze Block

Elements	Longbizui	Sancha	Rongxi (Gao et al., 2018)	Ganziping (Pan et al., 2004)	Lianxing (Jia et al., 2018)	Wenshui (Jia et al., 2018)	Yangtiao (Jia et al., 2018)	Jiumen (Jia et al., 2018)	Tanguanyao (Zhou et al., 2017)	Zouma (Zhou et al., 2017)
La	(10.9–57.2) 30.83(13)	(16.5–60.9) 25.05(14)	(2.72–344) 118.66(17)	(11.99–63.03) 24.08(19)	(24.06–35.10) 30.60(4)	(33.61–38.2) 35.60(5)	(1.22–26.24) 9.90(5)	(19.86–69.14) 41.34(4)	(16.3–39.6) 33.17(9)	(30.1–78.9) 50.71(14)
Ce	(10.2–83.1) 49.55(13)	(30.2–55.8) 42.05(14)	(2.31–339) 118.10(17)	(7.51–89.63) 46.61(19)	(33.2–64.8) 51.82(4)	(61.6–73.52) 69.74(5)	(0.8–38.4) 11.58(5)	(33.28–84.28) 61(4)	(29–75.7) 62.22(9)	(53.5–115) 77.61(14)
Pr	(1.94–14.4) 6.80(13)	(3.52–10.9) 5.07(14)	(0.71–74.8) 27.59(17)	(2.18–10.07) 5.53(19)	(3.8–7.8) 6.08(4)	(7.8–9.2) 8.68(5)	(0.16–4.62) 1.87(5)	(4.89–17.53) 9.70(4)	(3.54–9.31) 7.68(9)	(6.4–15.5) 10.54(14)
Nd	(7.71–61.4) 27.19(13)	(13.6–47.5) 20.34(14)	(3.4–331) 126.98(17)	(10.58–43.98) 21.61(19)	(10.75–30.65) 21.3(4)	(28.16–36.16) 33.15(5)	(0.86–17.28) 7.25(5)	(22.24–75.52) 39.18(4)	(13.4–36.1) 29.6(9)	(23.3–56.5) 39.58(14)
Sm	(1.59–13.5) 5.40(13)	(1.83–9.06) 3.83(14)	(0.7–76.2) 28.85(17)	(2.07–7.57) 3.64(19)	(1.28–6.60) 4.0(4)	(5.6–7.78) 6.47(5)	(0.33–3.84) 1.51(5)	(4.2–17.07) 8.03(4)	(2.55–6.99) 5.61(9)	(3.71–10.3) 7.08(14)
Eu	(0.61–4.92) 1.76(13)	(0.40–3.25) 0.94(14)	(0.1–21.5) 7.78(17)	(0.6–3.73) 1.01(19)	(0.24–1.24) 0.77(4)	(1.05–1.73) 1.31(5)	(0.17–3.56) 1.25(5)	(1.21–6.16) 2.70(4)	(0.54–1.37) 1.10(9)	(0.53–1.81) 1.16(14)
Gd	(1.52–14.8) 5.19(13)	(1.72–11.6) 3.99(14)	(0.8–86.7) 31.89(17)	(2.19–10.56) 4.09(19)	(1.12–6.03) 3.72(4)	(4.89–7.09) 5.82(5)	(0.38–4.55) 1.63(5)	(3.83–18.98) 8.26(4)	(2.34–6.33) 4.99(9)	(3.19–12.2) 6.27(14)
Tb	(0.26–2.77) 0.91(13)	(0.29–2.2) 0.75(14)	(0.17–14.9) 5.17(17)	(0.35–1.87) 0.72(19)	(0.23–1.07) 0.67(4)	(0.87–1.43) 1.02(5)	(0.06–0.83) 0.30(5)	(0.66–3.36) 1.47(4)	(0.42–1.12) 0.89(9)	(0.56–2.16) 1.09(14)
Dy	(1.55–17.5) 5.26(13)	(1.84–14.7) 4.65(14)	(1.1–87.9) 31.67(17)	(1.84–9.13) 3.74(19)	(1.54–4.97) 3.43(4)	(4.04–6.95) 4.94(5)	(0.35–4.79) 1.73(5)	(3.33–18.30) 7.76(4)	(2.37–5.96) 4.80(9)	(3.38–12.5) 6.02(14)
Ho	(0.35–3.68) 1.09(13)	(0.44–3.58) 1.04(14)	(0.26–16.7) 6.30(17)	(0.38–1.64) 0.72(19)	(0.38–1.04) 0.78(4)	(0.91–1.65) 1.11(5)	(0.10–1.18) 0.42(5)	(0.77–4.39) 1.83(4)	(0.58–1.15) 0.95(9)	(0.70–2.8) 1.22(14)
Er	(1.05–10.9) 3.18(13)	(1.41–10.3) 3.0(14)	(0.76–41.9) 16.53(17)	(1.23–5.63) 2.34(19)	(1.42–3.15) 2.39(4)	(2.34–4.58) 3.17(5)	(0.31–3.53) 1.30(5)	(2.43–11.80) 5.05(4)	(1.43–3.46) 2.75(9)	(2.02–8.31) 3.57(14)
Tm	(0.29–1.86) 0.55(13)	(0.27–1.67) 0.53(14)	(0.14–6.0) 2.57(17)	(0.24–0.8) 0.41(19)	(0.35–0.64) 0.52(4)	(0.5–0.93) 0.64(5)	(0.06–0.74) 0.26(5)	(0.47–1.99) 0.91(4)	(0.23–0.52) 0.45(9)	(0.36–1.29) 0.58(14)
Yb	(1.24–11.0) 3.40(13)	(1.79–9.35) 3.16(14)	(0.88–31.5) 14.25(17)	(1.36–3.71) 2.23(19)	(2.0–3.30) 2.72(4)	(2.57–5.01) 3.49(5)	(0.32–4.17) 1.45(5)	(2.60–8.44) 4.21(4)	(1.54–3.54) 2.86(9)	(2.38–7.24) 3.6(14)
Lu	(0.16–1.58) 0.48(13)	(0.27–1.28) 0.47(14)	(0.13–4.3) 1.92(17)	(0.23–0.46) 0.33(19)	(0.31–0.54) 0.45(4)	(0.42–0.82) 0.54(5)	(0.04–0.66) 0.23(5)	(0.44–1.2) 0.64(4)	(0.22–0.52) 0.42(9)	(0.32–1.06) 0.52(14)

Table 3 Continued

Elements	Longbizui	Sancha	Rongxi (Gao et al., 2018)	Ganziping (Pan et al., 2004)	Lianxing (Jia et al., 2018)	Wenshui (Jia et al., 2018)	Yangtiao (Jia et al., 2018)	Jiumen (Jia et al., 2018)	Tanguanyao (Zhou et al., 2017)	Zouma (Zhou et al., 2017)
Y	(13.8–115.0) 39.32(11)	(16.7–182.0) 41.32(14)	(9.4–755) 278.25(17)	(10.7–94.44) 24.96(19)	(11.1–31.8) 22.5(4)	(26.3–37.8) 32.24(5)	(4.05–44.6) 15.38(5)	(25.2–212) 80.58(4)	(13.8–34.3) 27.18(9)	(26.4–125) 40.5(14)
ΣREE	(58.66–395.61) 174.87(13)	(102.51–423.09) 156.20(14)	(14.3–1 470) 538.84(17)	(82.63–346.25) 142.06(19)	(79–164) 128.88(4)	(164–200) 180(5)	(7.52–97.9) 40.39(5)	(107–339) 190.75(4)	(88.28–227.14) 184.70(9)	(152.19–338.3) 250.03(14)
ΣLREE	(40.05–231.32) 126.73(13)	(71–133.78) 101.28(14)	(10.74–1 262.2) 460(17)	(38.38–228.57) 106.61(19)	(72.2–144) 114.28(4)	(147–171) 158.8(5)	(4.87–88.4) 33.29(5)	(87.3–272) 161.08(4)	(67.67–176.51) 144.40(9)	(107.08–284.41) 192.94(14)
ΣHREE	(4.81–49.29) 14.87(13)	(6.32–43.08) 13.60(14)	(3.44–202.8) 78.96(17)	(5.63–23.24) 10.50(19)	(7.29–20.8) 14.65(4)	(17.3–29.6) 21.4(5)	(1.74–19.8) 7.12(5)	(14.2–67.4) 29.6(4)	(6.80–16.33) 13.13(9)	(9.63–35.36) 16.60(14)
L/H	(2.48–14.99) 10.02(13)	(4.59–12.57) 8.31(14)	(3.12–15.46) 6.66(17)	(3.8–17.24) 10.54(19)	(6.92–9.90) 8.19(4)	(7.42–8.49) 7.61(5)	(1.83–9.26) 4.03(5)	(4.03–9.71) 6.67(4)	(9.32–12.74) 10.88(9)	(4.19–18.49) 12.91(14)
Y/Ho	(27.03–45.49) 34.54(11)	(32.80–50.83) 36.69(14)	(34–49.2) 41.47(17)	(25.77–57.58) 32.70(19)	(27.9–31.3) 29.52(4)	(22.5–34.2) 28.94(5)	(32.4–44.7) 38.5(5)	(33.4–50.5) 41.27(4)	(23.58–29.11) 28.24(9)	(27.53–30.96) 31.12(14)
La/Ce	(0.51–1.43) 0.69(11)	(0.49–1.11) 0.58(14)	(0.60–1.17) 0.96(17)	(0.43–1.59) 0.55(19)	(0.49–0.72) 0.62(4)	(0.47–0.54) 0.51(5)	(0.68–1.67) 1.11(5)	(0.59–0.81) 0.66(4)	(0.51–0.56) 0.53(9)	(0.56–1.23) 0.70(14)
Ce/Ce*	(0.30–0.90) 0.73(13)	(0.43–0.93) 0.86(14)	(0.36–0.78) 0.49(17)	(0.29–1.02) 0.91(19)	(0.78–0.92) 0.85(4)	(0.86–0.89) 0.87(5)	(0.36–0.79) 0.52(5)	(0.56–0.84) 0.74(4)	(0.85–0.89) 0.88(9)	(0.36–0.87) 0.75(14)
Eu/Eu*	(0.94–4.17) 1.77(13)	(0.93–1.47) 1.06(14)	(0.88–2.07) 1.34(17)	(0.98–1.94) 1.18(19)	(0.89–0.96) 0.93(4)	(0.94–1.11) 1.05(5)	(1.43–20.9) 5.99(5)	(1.25–1.83) 1.52(4)	(0.92–1.03) 0.97(9)	(0.48–1.02) 0.81(14)
Pr/Pr*	(0.98–1.18) 1.04(13)	(0.90–1.12) 0.97(14)	(0.98–1.21) 1.12(17)	(0.89–1.15) 0.99(19)	(0.99–1.14) 1.06(4)	(0.95–1.06) 1.02(5)	(0.96–1.21) 1.09(5)	(0.99–1.15) 1.07(4)	(0.99–1.02) 1.01(9)	(0.98–1.27) 1.08(14)
Y/Y*	(0.89–1.62) 1.19(13)	(1.12–1.87) 1.30(14)	(1.02–1.27) 1.17(17)	(0.80–1.66) 1.07(19)	(0.95–1.11) 1.04(4)	(0.83–1.20) 1.05(5)	(1.15–1.55) 1.40(5)	(1.17–1.77) 1.44(4)	(0.87–0.97) 0.94(9)	(0.89–1.60) 1.04(14)
$(La/Sm)_n$	(0.43–1.18) 0.88(13)	(0.75–1.75) 1.00(14)	(0.42–1.64) 0.71(17)	(0.64–1.35) 0.95(19)	(0.71–2.73) 0.77(4)	(0.63–0.88) 0.82(5)	(0.42–1.49) 0.78(5)	(0.53–1.28) 0.87(4)	(0.72–0.97) 0.86(9)	(0.70–1.31) 1.07(14)
$(Gd/Yb)_n$	(0.48–1.20) 0.93(13)	(0.49–0.86) 0.74(14)	(0.52–1.86) 1.16(17)	(0.87–1.69) 1.06(19)	(0.33–1.18) 1.49(4)	(0.84–1.13) 1.01(5)	(0.49–0.85) 0.70(5)	(0.87–1.33) 1.08(4)	(0.90–1.13) 1.04(9)	(0.82–1.20) 1.05(14)

4 DISCUSSION

4.1 Organic Geochemical Characterization

Organic carbon determines the quantity of TOC in sedimentary rocks (Awan et al., 2021a). Outcrop samples labelled as CR and LA were selected from two Sancha and Longbizui sections to determine total organic carbon which can be utilized to categorize the source rock quality, such as excellent >4.0 wt.%, very good 2.0 wt.%–4.0 wt.%, good 1.0 wt.%–2.0 wt.%, fair 0.5 wt.%–1.0 wt.%, and poor <0.5 wt.% (Peters and Cassa, 1994). The results show higher TOC quantities in the Sancha Section relative to the Longbizui Section. The comparison of TOC from lower to higher amounts relative to the other sections is as follows: Tanguanyao 0.30 wt.%, Zouma 1.5 wt.%, Lianxing 2.74 wt.%, Wenshui 3.11 wt.%, Longbizui 3.34 wt.%, Yangtiao 3.65 wt.%, Jiumen 4.7 wt.%, Ganziping 7.43 wt.%, Sancha 8.09 wt.%, Rongxi 8.65 wt.% (Table 1). This increasing trend reveals the content of total organic carbon in the Niutitang Formation is lower in the platform areas, whereas it increases towards the deep shelf and slope regions. Moreover, the TOC reveals the Niutitang Formation in the study area has good to excellent potential to produce hydrocarbons. At the same time, lower TOC values were encountered at the Tanguanyao Section, which suggests the Niutitang Formation deposited on the platform has a poor potential to produce hydrocarbons. In the studied sections, mainly four lithofacies were encountered. In these lithofacies, silty mudstone and siliceous rocks contain lower quantities of TOC, whereas the shales and mudstone facies contain higher quantities of total organic carbon (Fig. 2). In sediments, various factors such as transgression and regression of sea level, rapid sedimentation that could enhance the OM burial efficiency, upwelling, and anoxic setting, are factors that could increase the amount of TOC in the sediments (Yeasmin et al., 2017; Arthur and Sageman, 2005; Katz, 2005). The higher TOC quantities in these rocks could suggest the anoxic setting during the deposition of the Early Cambrian Niutitang Formation and inadequate bacterial action on the organic matter that could have eradicated organic matter to a certain extent (Loucks and Ruppel, 2007).

4.2 Inorganic Geochemistry

The pattern of REEs may be used to determine depositional processes, the architectural background of the basin, and the deposition environment of sediments. Geologists have devoted much attention to the pattern of rare earth elements from deep rift basins, marine basins, mid-oceanic ridges, and oceanic basins, particularly deep-seated sediments associated with hydrothermal activities. In clastic rocks, the chemical constituents are due to the net effect of various prevailing geological conditions. The following are the main factors: (i) composition of the source rock; (ii) disintegration of rock (weathering) both via chemical and physical agents; (ii) post-depositional weathering; (iv) sorting of sediments; (iv) sedimentation rate. These factors must be assessed before concluding the nature of the rock and the regional tectonics from the clastic rocks' composition. The abundance of REEs and Y in black rock sediments of the Niutitang Formation from the studied Longbizui and Sancha sections, and its comparison with different sections of South China Block are displayed in Table 3. These two studied

sections contain higher quantities of ΣREE compared to the Ganziping, Lianxing, and Yangtiao sections, whereas they contain lower quantities than those of the Rongxi, Wenshui, Jiumen, Tanguanyao, Zouma sections. Moreover, the Longbizui Section is enriched in the concentration of REEs comparative to the amount of global crust (146 ppm) (McLennan, 2001) and Post Australian Archean Shale (173 ppm) (Ma et al., 2017), North American Shale Composite (NASC 167.41 ppm) (Haskin et al., 1968), Chinese coals (162.51 ppm) (Dai et al., 2008), worldwide coals (34.1 ppm) (Valkovic, 1983) and world black shales (134.19) (Ketris and Yudovich, 2009). However, the ΣREEs of the Sancha Section are depleted relative to the amount of Post Australian Archean Shale (173 ppm) (Ma et al., 2017), North American Shale Composite (NASC 167.41 ppm) (Haskin et al., 1968), and Chinese coals (162.51 ppm) (Dai et al., 2008), while they are more enriched than those of worldwide coals (34.1 ppm) (Valkovic, 1983), world black shales (134.19 ppm) (Ketris and Yudovich, 2009), and global crust (146 ppm) (McLennan, 2001). The normalized pattern of REEs from various sections of the Niutitang Formation using PAAS reveals a slight inclination towards the left side with a negative Ce anomaly (Fig. 3a). Here in the black specimens of the Niutitang Formation, we have divided the sample/PAAS into three intervals (Figs. 3a–3c). (i) As the value of sample/PAAS is about 1.0, where REEs' distribution pattern is displaying a flat profile. This kind of flat profile in REEs is similar to that of seawater. (ii) As the amount of sample/PAAS is between 0.1–1.0 in this scenario, the REEs pattern is slightly tilting towards the left. This type of model reveals a lower concentration of LREEs with relatively higher enrichment of HREEs. (iii) In the third pattern, the concentration amount of sample/PAAS ranges between 1 to 10.0 due to the higher level of REEs. A couple of samples from both studied section present this kind of pattern. Generally, REEs' overall concentration in the Niutitang Formation is lower than the Post Australian Archean Shale, excluding the Rongxi Section (Fig. 3a).

4.3 Redox Conditions

Redox-sensitive trace elements such as V, Mo, and U, can be utilized to determine the paleoceanographic conditions. These susceptible elements are enormously enriched in redox settings, and their concentration can vary in anoxic conditions (Awan et al., 2020; Wu et al., 2020; Tang et al., 2017; Algeo, 2004). The trace elements pattern in the Niutitang Formation is useful in inferring paleo sedimentary settings. The average values of V/(V + Ni) from the Longbizui and Sancha sections are 0.83 and 0.77, respectively, indicating oxygen-deficient settings during the Niutitang Formation deposition. Ni/Co and V/Cr values in the studied samples are greater than 7.0 and 7.25, respectively. Similarly, the quantities of U/Th and δU are greater than 1.25 and 1.0. All samples studied show higher quantities of U/Th, Ni/Co, V/(V + Ni), and V/Cr (Table 4), which indicates the black rocks of the Niutitang Formation in the studied block was deposited under oxygen-deficient, anoxic and reducing condition consistent with previous researches (Awan et al., 2021b; Wu et al., 2020; Li et al., 2019; Zhang et al., 2019; Algeo and Maynard, 2008). Comparing these redox indicators with other sections revealed the Niutitang Formation in the
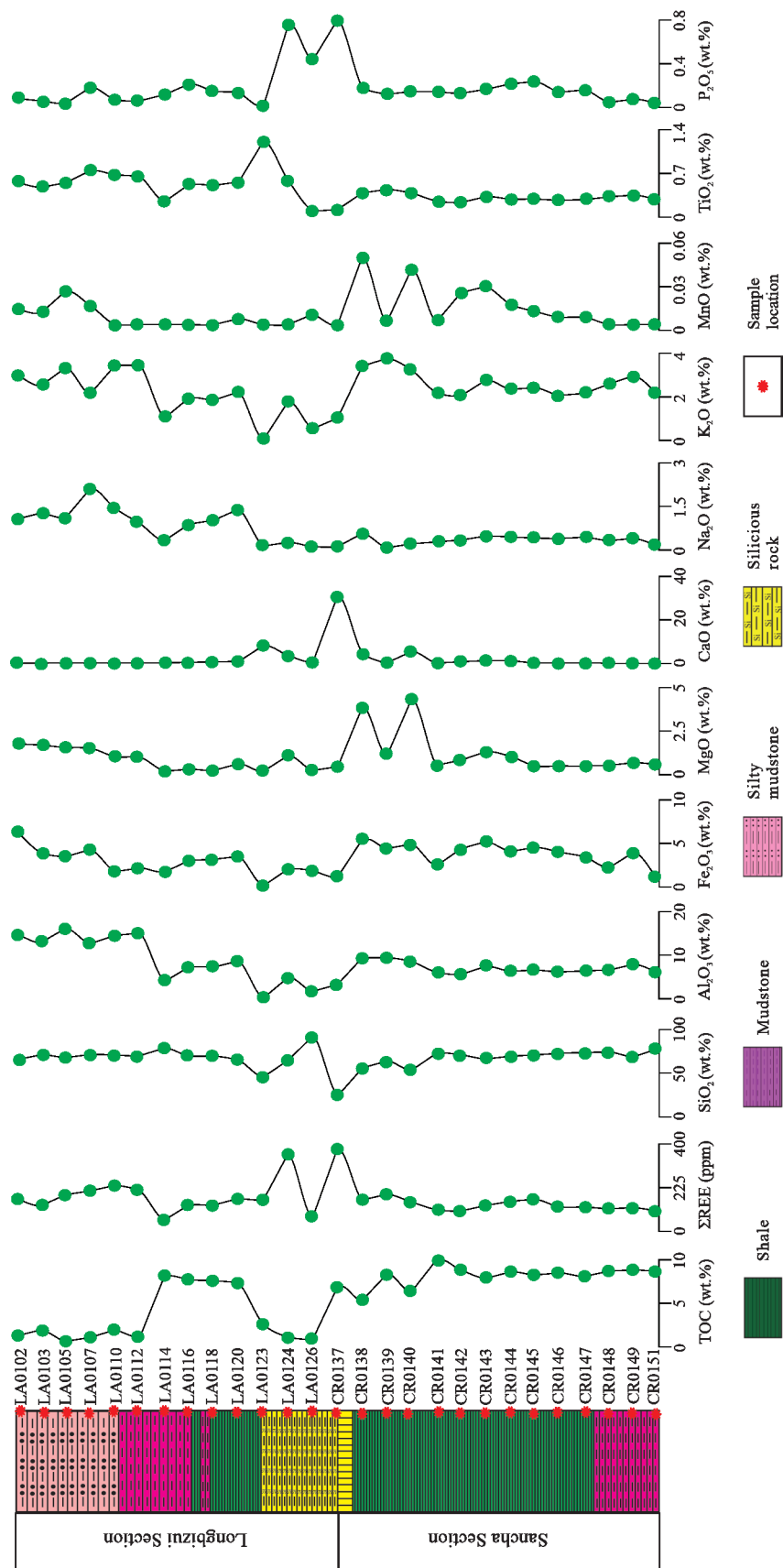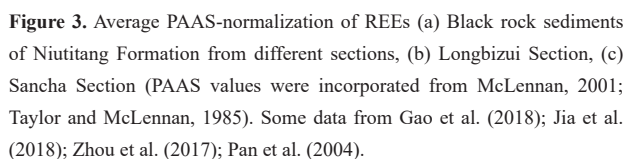
Figure 2. Vertical variation of TOC, REEs, and various trace elements from the Longbizui and Sancha sections.

Figure 3. Average PAAS-normalization of REEs (a) Black rock sediments of Niutitang Formation from different sections, (b) Longbizui Section, (c) Sancha Section (PAAS values were incorporated from McLennan, 2001; Taylor and McLennan, 1985). Some data from Gao et al. (2018); Jia et al. (2018); Zhou et al. (2017); Pan et al. (2004).

Table 4 Characteristics of redox-sensitive trace elements in the anoxic setting

Sedimentary environmental indicators	Anoxic environment		Oxygen-rich environment	Longbizui	Sancha	Rongxi (Gao et al., 2018)	Ganziping (Pan et al., 2004)	Tanguanyao (Zhou et al., 2017)	Zouma (Zhou et al., 2017)
	Anaerobic	Oxygen deficient							
V/(V + Ni)	>0.54	>0.46–0.60	<0.46	(0.61–0.94) 0.83(11)	(0.70–0.92) 0.77(13)	(0.39–0.98) 0.86(17)	(0.12–0.97) 0.74(19)	(0.50–0.82) 0.71(9)	(0.64–0.91) 0.78(14)
V/Cr	>4.25	>2.0–4.25	<2.0	(0.99–23.60) 6.14(11)	(3.73–13.66) 7.32(13)	(0.94–28.89) 8.91(17)	(0.94–12.78) 5.69(19)	(0.42–2.69) 1.38(9)	(0.63–1.21) 0.91(14)
Ni/Co	> 7.0	4.0–7.0	<4.0	(1.98–36.57) 13.26(11)	(4.09–64.71) 12.13(13)	-	(0.97–6.17) 5.05(19)	(2.56–7.16) 3.70(9)	(2.11–26.68) 8.74(14)
U/Th	>1.25	0.75–1.25	<0.75	(0.31–33.15) 7.08(11)	(5.53–11.81) 9.05(14)	(0.27–101.85) 18.21(17)	(1.14–67.71) 18.17(19)	(0.20–0.54) 0.40(9)	(0.16–8.46) 1.37(14)
δU	>1.0		<1	(0.96–1.98) 1.64(11)	(1.89–1.95) 1.93(13)	(0.90–1.99) 1.86(17)	(1.55–1.99) 1.88(19)	(0.78–1.24) 1.07(9)	(0.66–1.92) 1.09(14)

Tanguaoyang Section on the platform region was deposited in relatively oxic condition. In the studied samples, the enrichment factor of Cs is greater than 1, whereas Rb is depleted. However, a crossplot between Rb/Cs and Rb/K reveals a positive relationship (Fig. S2). Cs and Rb trace elements are large ion lithophile elements (LILEs) (Pan et al. 2004). These marine sediments could have been deposited in a detrital phase and vary as abiogenic elements or mixed dilution of detritus (Plank and Langmuir, 1998). Additionally, Zr, Hf, Ta, and Nb are con-

sidered high field strength elements (HFSEs) (Pan et al., 2004). Nb/Ta and Zr/Hf's relationship reveals a positive relationship (Figs. S2c, S2d), while their enrichment factors are lower than 1.0. These results show the HFSEs in the Niutitang Formation might be diluted by biogenic elements. Both LILEs and HFSEs suggest the effect of detrital input is significantly lower on the concentration of trace elements. Paleo sedimentary settings influenced by post diagenetic process can be predicted by Ce anomalies (Shields and Stille, 2001; Wilde et al., 1996; German and Elderfield, 1990) which can also be used to determine and predict the variation in redox settings (Jia et al., 2018; Wilde et al., 1996). It was first used by Elderfield and Greaves (1982) due to an alteration in Ce ionic state based on oxidation. The ratio of Ce/Ce* was used to estimate the Ce anomaly. The Ce element has two valence variants, Ce^{3+} and Ce^{4+}, and Ce^{3+} can shift to Ce^{4+} in oxidation settings. In this paper, Ce is the concentration of Ce in Niutitang Formation (Ce_{Niu}) divided by the value of Ce in the upper continental crust (Ce_{Niu}/Ce_N), and Ce* is acquired by incorporating the normalized amount of La and Pr. It can be used to distinguish the loss and enrichment of Ce and to determine the oxic and anoxic setting of paleo-ocean. A loss of Ce anomaly causes positive and negative anomalies in sediments and in water, respectively. In oxidizing settings, a few oxides (Mn and Fe) quickly adsorb Ce and consequently, Ce becomes isolated from other REEs. Thus, the Ce loss in seawater unveils a negative anomaly, whereas its enrichment in sedimentary rocks displays a positive Ce anomaly or no substantial negative Ce anomaly (≥ 1). Moreover, the fractionation of Ce from the other REEs could take place due to dwindling solubility and oxidation of Ce^{3+} to Ce^{4+} (Sholkovitz et al., 1994). Besides redox settings, the Ce behavior could be affected by water depth, pH, the age of the water body, and the microbial actions (German and Elderfield, 1990; Moffett, 1990). Conversely, the dissolution of Fe oxides in anoxic settings of ocean water or in sediments results in a positive anomaly and a negative Ce anomaly (<1), respectively. Moreover, if Ce is triggered and liberated in the form of Ce^{3+} into the water and thus in sediments and seawater, it will show a negative and positive Ce anomaly, respectively (Morad and Felitsyn, 2001). A significant number of samples containing Ce anomaly over 0.65 exhibit weak negative anomaly, whereas one particular specimen keeps lower values (<0.50), revealing a more robust negative Ce anomaly. In contrast, a few samples from the Ganziping Section show a weak positive Ce anomaly. In contrast, the average Eu anomaly quantities from Lianxing, Tanguanyao, and Zouma sections are unexpectedly lower than 1.0 (Table 3). Based on smaller to more significant Ce anomaly, the studied sections are classified as Rongxi (0.49) < Yangtiao < (0.52) < Longbizui (0.73) < Jiumen (0.74) < Zouma (0.75) < Lianxing (0.85) < Sancha (0.86) < Wenshui (0.87) < Tanguanyao (0.88) < Ganziping (0.91) (Table 3). These outcomes reveal a higher reducibility at the Rongxi area located on the deep shelf (Fig. 1). The sections with higher reducing settings were situated near or on the deep shelf/slope areas during sedimentation in the Cambrian period. The negative Ce anomalies with reducing conditions in these zones might be influenced by the depth of ocean water and hot subsurface fluids' activity. The Niutitang Formation in the Ganziping Section area was de-

posited in less reducing conditions similar to the Australian Heartherdale Shale, Emu Bay Shale, and Talisker Formation. Additionally, the Niutitang Formation in the Rongxi Section area was deposited in higher reducing conditions similar to the Tal Formation from India (Fig. S3). In the upper parts of the Longbizui, Sancha, and Zouma sections, the reducibility is relatively weaker as compared with the lower section, which might be due to hydrothermal activity. Submarine magmatic actions created numerous deep faults providing massive organic-rich nutrients in the form of various elements, developed not only in reducing settings, and provided heat for the Cambrian Explosion. In these circumstances, local anoxic settings were developed, and numerous quantities of OM deposited. Therefore, it is suggested that the redox setting could be controlled by various factors such as massive quantities of OM, hydrothermal activities, and variations in seawater depth. In the sediments, the enrichment of Ce varies with redox settings and the sedimentary environment. The amount of La/Ce in prehistoric ocean water or in the hydrothermal crust is around 2.8, deprived of Ce enrichment. In hydrogenetic rocks (containing Mn-Fe), the ratio is far lower, nearly 0.25, with an apparent advancement of cerium. The quantity of La/Ce in the studied section ranges of 0.49–1.43. However, significantly higher La/Ce values were noticed at the Yangtiao and Rongxi areas 1.11 and 0.96, respectively (Table 3). As the ratio (La/Ce) declines, the enrichment of Ce increases progressively (Fig. S3b). Moreover, if there is no relationship between Ce/Ce* and La_n/Sm_n ratios, it is possible to determine the primary Ce anomaly (Morad and Felitsyn, 2001). Additionally, iagenetic phenomena may produce a positive association between REEs and Ce anomaly and a negative linkage between Dy_n/Sm_n and Ce anomaly (Shields and Stille, 2001). In the studied samples, we have noticed a relatively positive linkage between Ce anomaly and La_n/Sm_n. A weak linkage exists between the REEs and Ce anomaly and a negative linkage between Dyn/Smn and Ce anomaly. Similarly, the relationship of Ce anomaly and the PASS normalized values La_n/Nd_n, Y/Y*, and Eu anomaly reveal no relationship (Figs. 4a, 4e, 4f). It is debatable, either the Eu anomaly altered or not throughout diagenesis. However, these relationships exhibit alteration of Ce anomaly during diagenesis.

The quantity of Eu may easily be enriched in sediments affected by hydrothermal activity or by reducing settings. Eu in magmatic and high calcium minerals such as potash feldspar and plagioclase may vary via substitution of Sr^{2+} by Eu^{2+} held by the identical ionic frameworks. In marine settings where reducing sulfates and high organic carbon are located, Eu^{3+} may presumably be reduced to Eu^{2+} by diagenesis. The relationship between the Eu anomaly and Ba can be utilized to indicate the ancient sedimentation setting due to the value of BaO/BaOH, which can be attributed to a linear association between Ba/Eu (Dulski, 1994). The specimens in the Niutitang Formation show no clear association of Eu anomaly with Sr and Ba (Fig. S4) that might provide preliminary information and clues to the presence of ocean water. A significant proportion of Ba in sediments or in water bodies signifies higher biological productivity. The disintegration of organic matter (OM) under anoxic settings may result in barite precipitation on organic particles.
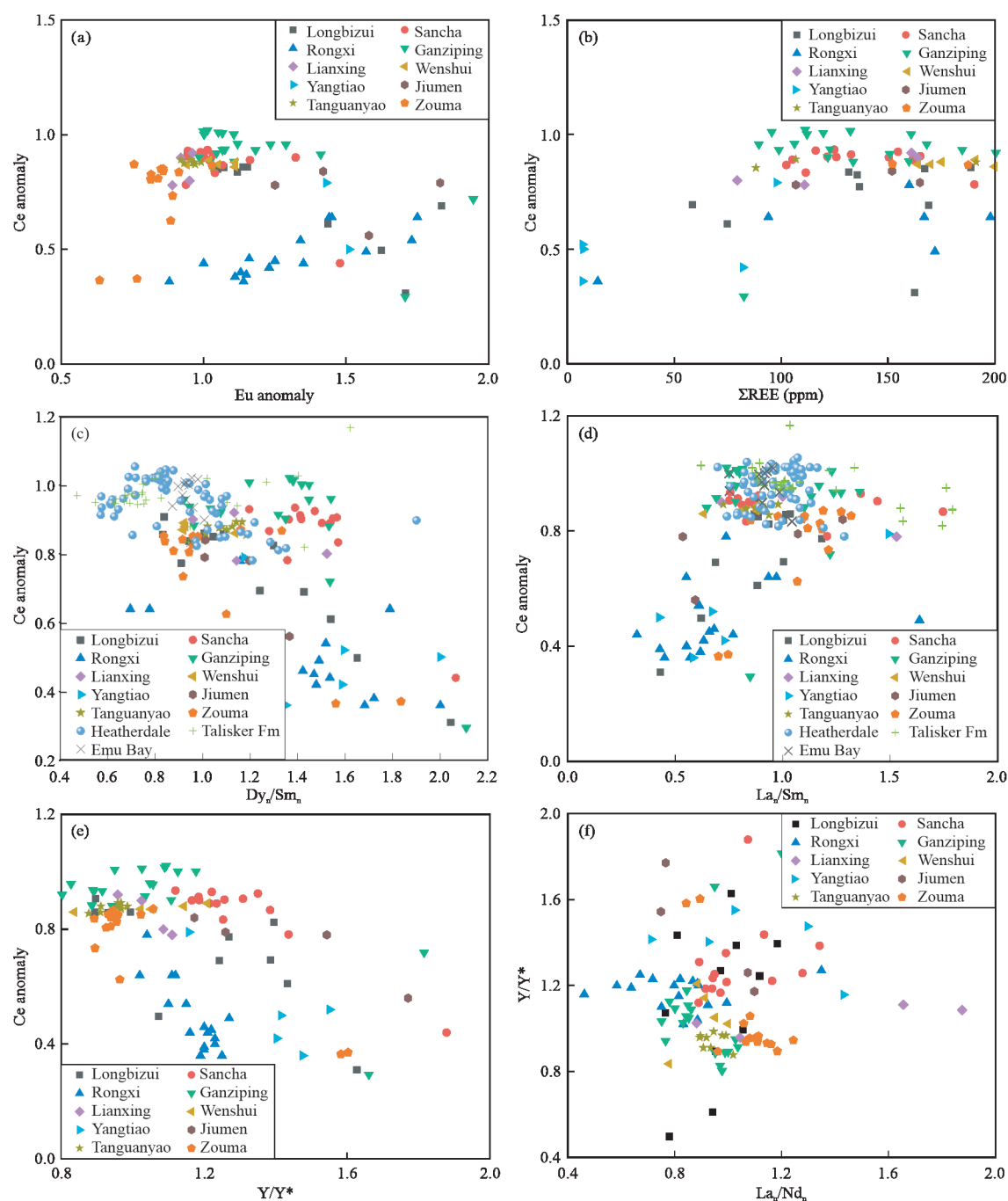
Figure 4. The scattered diagrams revealing the characteristics of rare earth elements (REEs). Some data from Gao et al. (2018); Jia et al. (2018); Zhou et al. (2017); Hall (2012); Pan et al. (2004).

4.4 Effect of Hydrothermal Activity

Hydrothermal actions indicate reducing settings and therefore hydrothermal activities are key for predicting reducing conditions (Steiner et al., 2001). A normal depositional rate of 10 cm/ka or a faster depositional rate of 40 cm/ka is viable for the deposition of massive quantities of hydrothermal sediments in a short period (Li et al., 2013). Therefore, several elements could be enriched in sediments associated with hydrothermal sedimentation (Marchig et al., 1982; Rona, 1978). Antimony (Sb) commonly prevails in hydrothermal fluids and magmas and is considered an indicator element for hydrothermal sedimentation. The enrichment factor of Sb could be utilized to pre-

dict sediments that are affected by hydrothermal activities. The enrichment factor of Sb from the studied Longbizui and Sancha sections falls in the range of 1.5–3.64 and 8.76–48.0, respectively. These results reveal the Niutitang Formation is highly affected by hydrothermal activities. The distributions of rare earth elements in rocks are used to determine the nature of sedimentation and provenance (Zhu et al., 2014; Uysal et al., 2007). The chemical and geological behaviors of REEs may reveal an understanding of geochemical progressions that happened through the sedimentation period. The various diagenetic process can be predicted by incorporation of the relationship between REEs and the ratio of La/Yb (Allegre and Michard,

1974) and Ce/La vs. La/Yb (Yang et al., 2011). Most of the samples in the study area reveal an association with basalts or their equivalents, and some from granites. These results inicate a typical marine setting, influenced by a deep hot water activity during the sedimentation process (Figs. 5a, 5b). The positive Eu anomalies during diagenesis are usually related to extreme reducing settings (Kidder et al., 2003; Ogihara, 1999). In these settings, the decomposition of OM would devour the existing oxygen, which causes the reduction of Eu^{3+} to Eu^{2+}. Later due to phosphates, the Eu^{2+} may be scavenged and develop a positive Eu anomaly. The ratio of Eu/Eu* was used to estimate the Eu anomaly. Here Eu is the concentration of Eu in the Niutitang Formation (Eu_{Niu}) divided by the frequency of Eu in the upper continental crust (Eu_{Niu}/Ce_N), and Eu* is acquired by incorporating the normalized amount of Sm and Gd. The Eu anomaly has a close relationship with ambient temperature and can be utilized to discriminate natural and hydrothermal sediments. A positive Eu anomaly specifies a medium-higher thermal degree of sedimentary settings for sediment deposition (temperature higher than 250 °C) most frequently related to hot water fluids associated with MOR (mid-oceanic ridges) or with back-arc basin. In shallow seawater, a positive Eu anomaly may not be an indicator of reducing conditions (Kamber and Webb, 2001). Negative and no anomalies are a sign of natural sediments and intermediate to lower thermal degree of sedimentation (temperature lower than 250 °C), respectively (Jia et al., 2018; Schijf et al., 1991).

In the study area, the Eu anomaly from the Longbizui and Sancha sections is 1.77 and 1.07, respectively, revealing a positive Eu anomaly. In contrast, the average Eu anomaly values from Lianxing, Tanguanyao, and Zouma sections are unexpectedly lower than 1.0 (Table 3). The maximum specimen exhibits a positive Eu anomaly except for the samples of Zouma Section with weak negative anomaly designates typical marine sedimentation or not affected by hot water fluids (Fig. S5). The Lianxing and Tanguanyao overlap with the Niutitang Formation, Emu Bay Shale, the lower part of the Heatherdale Shale, Talisker, and Tal Formation in showing weak negative or no Eu anomaly as a sign of natural sediments, and intermediate to

lower thermal degree of sedimentation. Throughout the Ediacaran and Early Cambrian rocks of the Yangtze region, a slightly positive Eu anomaly has been observed (Tian and Luo, 2017; Guo et al., 2007). This might be due to weaker hot water phenomena, or that the hydrothermal activity's focal point was far away from these zones. The weaker negative Eu anomaly indicates that sedimentary deposits aren't instantly affected by the hydrothermal flux. The combination of seawater and hydrothermal fluids may develop a weak positive Eu anomaly associated with authigenic deposits. Eu^{2+} in euxinic settings could be stable as in the modern Black Sea. Strong positive anomalies in the Longbizui, Sancha, Yangtiao, Jiumen, Rongxi, and Ganziping sections and the upper part of Heatherdale Shale, Talisker, and Tal formations could be due to significant hydrothermal action during their deposition in the Cambrian period. This scenario suggests that the subsurface source of hydrothermal fluids is most likely associated with a mantle plume that could be between the Rongxi, Longbizui, Ganziping, and Yangtiao sections areas. Liu et al. (2016) and Awan et al. (2020) suggested the submarine hot water fluids related to volcanic plumes or with hydrothermal activities may deposit metallic ores on the seabed. Therefore, we still need to find a commercial polymetallic deposit in the study area as it is thought that hydrothermal events profoundly influenced the Niutitang Formation. Previous research suggested submarine rocks influenced by hydrothermal intrusion contained a higher concentration of Zn and Ba. The U/Th factor is critical in reflecting the characteristics of such a rock. For instance, the quantity of U/Th for a typical sedimentary setting is lower than 1, whereas it is over 1 in those rocks that are affected by deep mantle hydrothermal activities. Most of the specimens from the black rocks of the Niutitang Formation lie within the range 1.0–100 (Fig. 6a), which also is a close characteristic of hydrothermal imprint deposition. In the Tanguanyao and Zouma sections, the ratio is 0.1–1.0 and is a clue to normal marine condition beyond the hotspot zone range. Trace elements such as Co, Cu, and Ni are poorly enriched in rocks interacting with deep hot water fluids relative to hydrogenous rocks. Similarly, these values are lower in the East Pacific Rise (EPR) and higher in typical marine sediments. The enrich-
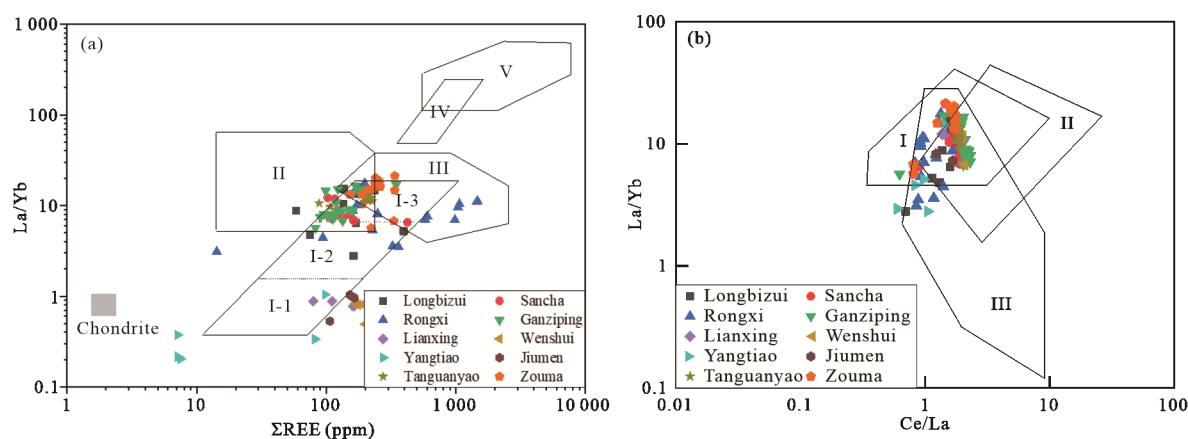

Figure 5. (a) Diagram showing the relationship between La/Yb and ΣREE (modified after Allegre and Michard, 1974); I-1. oceanic basalt; I-2. continental tholeiitic; I-3. alkali basalt; II. sedimentary rocks; III. granite; IV. kimberlite; V. carbonatite. (b) Diagram showing the association of La/Yb with Ce/La (modified after Yang et al., 2011); I. deeper ocean sedimentation; II. ferromanganese nodules and ferromagnesian rocks; III. submarine basaltic rocks, and their equivalent. Some data from Gao et al. (2018); Jia et al. (2018); Zhou et al. (2017); Pan et al. (2004).

ment of these elements (Co, Cu, and Ni) in ferromanganesian rocks indicates a lower deposition rate and the absorption capacity of transition elements in ocean water. The proportional discrepancies in the concentration of Zn and Co may better discriminate the genesis of diverse rocks, e.g., the ratio of Co/Zn can differentiate sediments related to deep hot water activities and typical authigenic sediments (Choi and Hariya, 1992). A positive Eu anomaly except for the Zouma Section sample with a weak negative anomaly designates typical marine sedimentation or deposition not affected by hot water fluids (Fig. S5). That the Lianxing and Tanguanyao sections comprising the Niutitang Formation, Emu Bay Shale, the lower part of the Heatherdale Shale, Talisker, and Tal Formation show weak negative or no Eu anomalies as a sign of natural sediments, and intermediate to lower thermal degree of sedimentation. Throughout the Ediacaran and Early Cambrian rocks of the Yangtze region, a slightly positive Eu anomaly has been observed (Tian and Luo, 2017; Guo et al., 2007). It might be due to weaker hot water phenomena, or the hydrothermal activity's focal point was far away from these zones. The weaker negative Eu anomaly states that sedimentary deposits aren't instantly affected by the hydrothermal flux. The combination of seawater and hydrothermal fluids may develop a weak positive Eu anomaly associated with authigenic deposits. The positive Eu anomaly except for the samples of Zouma Section with weak negative anomaly designates typical marine sedimentation or not affected by hot water fluids (Fig. S5). Lianxing and Tanguanyao section comprising Niutitang Formation, Emu Bay Shale, the lower part of the Heatherdale Shale, Talisker, and Tal Formation shows weak negative or no Eu anomaly is a sign of natural sediments, and intermediate to lower thermal degree of sedimentation. Throughout the Ediacaran and Early Cambrian rocks of the Yangtze region, a slightly positive Eu anomaly has been observed (Tian and Luo, 2017; Guo et al., 2007) which might be due to weaker hot water phenomena, or that the hydrothermal activity's focal point was far away from these zones. The weaker negative Eu anomaly shows that sedimentary deposits aren't instantly affected by hydrothermal flux. The combination of seawater and hydrothermal fluids may develop a weak positive Eu anomaly

associated with authigenic deposits. The Eu^{2+} in euxinic settings could be stable suchlike in the modern Black Sea. A vigorous positive anomaly in the Longbizui, Sancha, Yangtiao, Jiumen, Rongxi, and Ganziping sections and the upper part of Heatherdale Shale, Talisker, and Tal Formation could be due to significant hydrothermal action during their deposition in the Cambrian period. This scenario suggests that the subsurface source of hydrothermal fluids most likely associated with a mantle plume could be between the Rongxi, Longbizui, Ganziping, and Yangtiao section areas. Liu et al. (2016) and Awan et al. (2020) suggested the submarine hot water fluids related to volcanic plumes or with hydrothermal activities may deposit metallic ores on the seabed. However, we still need to find a commercial polymetallic deposit in the study area as it is thought that hydrothermal events profoundly influenced Niutitang Formation.

Previous research has suggested the submarine rocks influenced by hydrothermal intrusion contain a higher concentration of Zn and Ba. The U/Th factor is critical in reflecting the characteristics of a rock. For instance, the value of U/Th for a typical sedimentary setting is lower than 1, whereas it is over 1 in those rocks that are affected by deep mantle hydrothermal activities. Most of the specimens from the black rocks of the Niutitang Formation lie within the range 1.0–100 (Fig. 6a), which also reflects a characteristic of hydrothermal imprint deposition, but in the Tanguanyao and Zouma sections, the ratio is 0.1–1.0 and is a clue to normal marine conditions beyond the hotspot zone range. Trace elements such as Co, Cu, and Ni are poorly enriched in rocks interacted with deep hot water fluids relative to hydrogenous rocks. Similarly, these values are lower in the East Pacific Rise (EPR) and higher in a typical marine sediment trap. The enrichment of the elements Co, Cu, and Ni in ferromanganesian rocks indicates a lower deposition rate and the absorption capacity of transitional elements in ocean water. The proportional discrepancies in the concentration of Zn and Co may better discriminate the genesis of diverse rocks, e.g., the ratio of Co/Zn can differentiate sediments related to deep hot water activities and typical authigenic sediments (Choi and Hariya, 1992). The crossplot between Co/Zn vs. (Cu + Co + Ni) reveals (Fig. 6b) all the available Niutitang Forma-
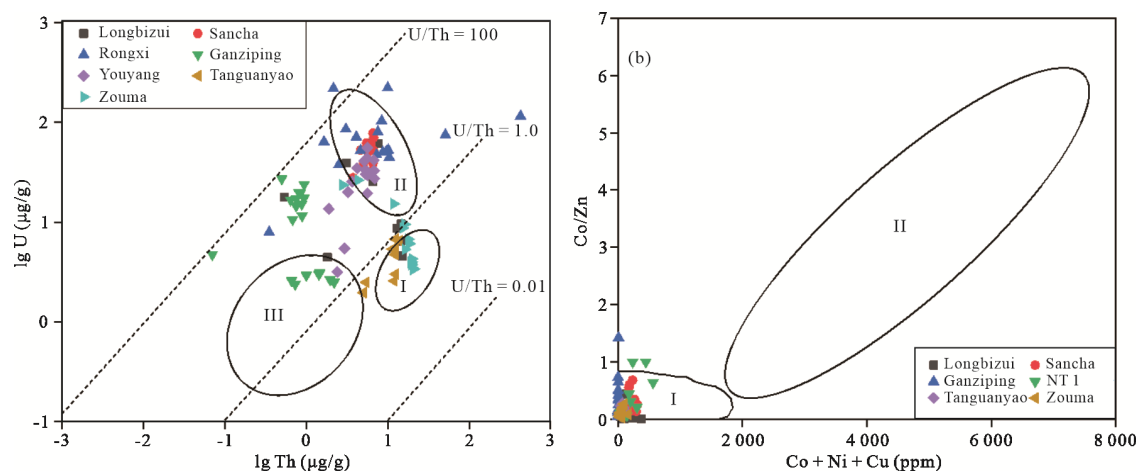

Figure 6. (a) Diagram showing the relationship between Th vs. U (modified after Yang et al., 2011); I. normal ocean sedimental trap; II. East-Pacific Rise (EPR); III. hydrothermal activity related sediments. (b) Diagram showing the relationship between Co/Zn vs. Co + Ni + Cu; I. hydrothermal sediments; II. hydrogenous sediments. Some data from Gao et al. (2018); Zhou et al. (2017); Tuo et al. (2016); Wu et al. (2016); Pan et al. (2004).

tion samples are highly affected by deep submarine hydrothermal actions. The typical praseodymium (Pr) anomaly in the studied Longbizui and Sancha sections are 1.04 and 0.97, respectively. Bau and Dulski (1996) suggested the higher content of La could also exaggerate the negative Ce anomaly. There we also used the Bau and Dulski (1996) method to evaluate the degree of La enrichment. Most of the specimens in the bivariant Ce/Ce vs. Pr/Pr graph fall within the zone IIa, while the selected samples from Australia and India are in region I (Fig. 7a). These results reveal that neither enrichment in La nor Ce signifies an increase of the La anomaly indicated by a negative Ce anomaly. However, Cambrian samples from Australia and India might exhibit a weak positive Ce anomaly due to the enrichment of La (Shields and Stille, 2001). Holser (1997) also suggested the negative Ce anomaly in the modern ocean is due to the enrichment of intermediate rare earth elements. The crossplot between Dy_n/Sm_n and Ce anomaly of the Niutitang samples displays no relationship, suggesting the negative Ce anomaly is insignificantly influenced by the mid-rare earth elements (MREEs) (Fig. 7b). Generally, these black sediments have an actual negative Ce anomaly instead of La or midrare earth elements enrichment. Usually, these black sediments in euxinic settings could be stable suchlike in the modern Black Sea. Strong positive anomalies in the Longbizui, Sancha, Yangtiao, Jiumen, Rongxi, and Ganziping sections and the upper part of Heatherdale Shale, Talisker, and Tal Formation could be due to significant hydrothermal action during their deposition in the Cambrian period. This scenario suggests that the subsurface source of hydrothermal fluids most likely associated with a mantle plume could be between the Rongxi, Longbizui, Ganziping, and Yangtiao sections areas. Liu et al. (2016) and Awan et al. (2020) suggested the submarine hot water fluids related to volcanic plumes or with hydrothermal activities may deposit metallic ores on the seabed. Therefore, we still need to find a commercial polymetallic deposit in the study area as it is thought the hydrothermal events profoundly influenced the Niutitang Formation.

4.5 Degree of Weathering and Source Rock Composition

The chemical compounds in rocks commonly represent their major mineral contents. In numerous instances, these chemical compounds are readily altered by chemical weathering (Ding et al., 2018). The cations of certain elements such as Mg, Al, Rb, and Cs are typically more resistant to chemical weathering than other elements with slightly small atomic radii such like K, Ca, and Na, that can quickly wash out in a dissolved state (Kasanzu et al., 2008). The percentage of elements lost is relative to the grade of weathering (Condie, 1993). Lutites are chiefly comprised of finegrained particles of silicate minerals as in clays and silts. Their degree of weathering can be determined using the chemical index of alteration and weathering (CIA and CIW). These indexes are measured as follows

$$CIA = \left(\frac{Al_2O_3}{CaO* + Al_2O_3 + Na_2O + K_2O} \right) \times 100 \qquad (i)$$

$$CIW = \left(\frac{Al_2O_3}{CaO* + Al_2O_3 + Na_2O} \right) \times 100 \qquad (ii)$$

The units used for these major elemental oxides in the above equations is mol proportion. The amount of CaO* in these equations is acquired from silicates (Nesbitt and Young, 1982). In this context, there is a need to calibrate the estimated content of CaO for the amounts of carbonate minerals. CaO is mainly correlated with phosphate in the current research via the assessed amount of P_2O_5 (McLennan et al., 1993).

$$CaO* = CaO - \left(P_2O_5 \times \frac{10}{3} \right) \qquad (iii)$$

If the residual mol quantity is less than Na_2O, then the mol quantity of CaO can be defined as CaO*. If not, then the mol proportion of CaO is thought correspond to Na_2O (Tang et al., 2018; Bock et al., 1998). The studied specimens are mainly comprised of quartz and clay minerals. Therefore, CIW and CIA can be utilized to illustrate the degree of weathering in these samples. The quantities of CIW and CIA in the Niutitang Formation are presented in Table 2. In the studied samples, the
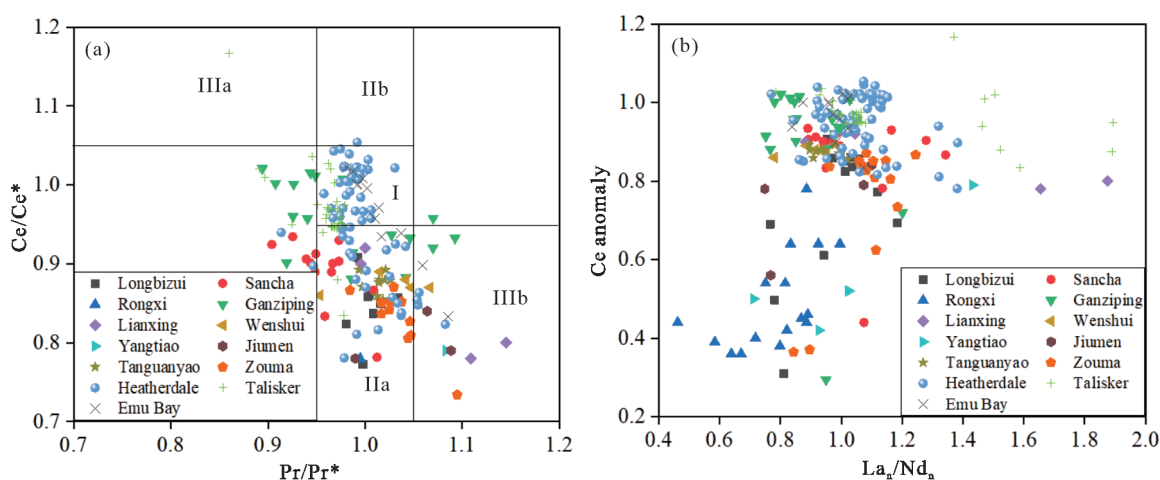

Figure 7. (a) The crossplot between Pr/Pr* and Ce/Ce* displaying a positive La anomaly. Pr anomaly (Pr/Pr*) and Ce anomaly (Ce/Ce*) were calculated by $2Pr_N/(Ce_N + Nd_N)$ and $3Ce_N/(2La_N + Nd_N)$ according to Shields and Stille (2001); I. neither Ce nor La anomalies; IIa. positive La anomaly leads to negative Ce anomaly; IIb. negative La anomaly leads to positive Ce anomaly; IIIa. positive Ce anomaly, IIIb. negative Ce anomaly. (b) The relationship between Ce-anomaly vs. La_n/Nd_n in Niutitang Formation. Some data from Gao et al. (2018); Jia et al. (2018); Zhou et al. (2017); Hall (2012); Pan et al. (2004).

values of CIA fluctuate between 61.33 and 79.46, with a mean of 71.32. The value of the CIA in the Niutitang Formation is relatively higher than the CIA quantity in PAAS (69), indicating a more weathered source than PAAS. Figure 8a displays the relationship of Al/Na with CIA, which indicates moderate weathering even though the black rocks of Niutitang Formation are composed of shale, siltstone, and mudstone. This might be due to diagenetic reduction of Na ions (Kasanzu et al., 2008). Moreover, CIW values that range from 71.91 to 98.61, averaged at 88.24, are analogous to CIA in the studied sections. Both the chemical index of weathering and chemical index of alteration show these black sediments might be from moderately weathered sources. The occurrence of major elements in a rock such as shale or mudrock reveals its transformation over time, mainly diagenetic and metamorphic changes. Existing chemical compounds can indicate a novel mineralogic composition in shales. For this purpose, the proportional ratio of K_2O/Al_2O_3 and the index for compositional variability [ICV = $(K_2O + CaO + Fe_2O_3 + TiO_2 + Na_2O + MgO)/Al_2O_3$] can be used. Clay minerals compared with non-clay minerals have a lower proportion of major cations to Al_2O_3 and therefore, the clay minerals usually have a depleted ICV. For example there is an increasing order of ICV in kaolinite (~0.03–0.05), montmorillonite (~0.15–0.3), illite and muscovite (~0.3), plagioclase (~0.6), alkali feldspar (~0.8 – 1.0), biotite (~0.8), and amphibole and pyroxene (~ 10–100) (Cox and Lowe, 1995). Immature shales with a higher percentage of non-clays usually have a higher ICV > 1. Shale with higher ICV normally exists in active tectonic regions in a first cycle deposit. On the other hand, clay-rich matured mudrocks normally have a lower ICV content (<1), which is thought to be usually formed in cratons of quiescent settings, which have also been identified in intensely weathered first cycle matter. The content of ICV in Niutitang Formation in the studied region ranges of 0.49–1.69 with a mean value of 1.01. These results reveal the Niutitang Formation is moderately weathered and are first cycle deposits of an active tectonic area. In original rock sediments, the actual amount of alkali feldspar vs. clays/plagioclase minerals is determined by using the ratios of K_2O/Al_2O_3. Lower to higher values of the K_2O/Al_2O_3 ratio of

minerals are as follows; clay minerals (~0), illite (~0.3), but alkali-felspars normally have (~0.4–1.0) (Cox and Lowe, 1995). In shales, higher ratios of K_2O/Al_2O_3 (>0.5) indicate a substantial amount of alkali-feldspar relative to other minerals. In contrast, lower ratios of K_2O/Al_2O_3 (<0.4) in original rock sediments are an indication of a normal concentration of alkali-feldspar. The ratio of K_2O/Al_2O_3 in black sediments of Niutitang Formation varying of 0.15–0.48 with a median amount of 0.27 reveals the minimum concentration of alkali-feldspar with respect to other minerals. Additionally, we can determine the components of the source sediments by displaying the molar ratios of K_2O-$(Na_2O + CaO)Al_2O_3$ in a ternary graph. This plot indicates diagenesis/metamorphism, transportation, composition, and intensity of chemical weathering (Fedo et al., 1997, 1995), provided that extensive compositional data of sandstone or shale are available to plot in the A-CN-K ternary graph. It can then be used to infer the mean compositional compounds and the metasomatic effect of the source sediments. In this type of ternary plot, if the specimens settle parallel to the A-CN line, it indicates a weathering mechanism. The initial phase of chemical weathering starts with the hydrolysis of plagioclase. It leads to the development of kaolinite that lies at the apex of A (Fig. 8b). Thus specimens that have been affected by chemical weathering would have a more significant amount of aluminum and will fall at the apex of A corresponding to the A-CN limit. Owing to K-metasomatism, weathered sediments of kaolinite may lead to illitic shale if the sample data fall perpendicular to the A-K boundary (Fig. 8b). According to the ternary plot, some specimens of the Niutitang Formation fall along the A-K line revealing moderate chemical weathering and high CIA. Conversely, half of the examined specimens are parallel to the A-CN boundary revealing these sediments have been affected by K-metasomatism. These sediments might originate from tonalite-basalt. As the sediments are moderately weathered, it suggests these rocks might have been derived from felsic rocks, mainly from granite-granodiorite. Similarly, the lower ratios of K_2O/Al_2O_3 indicate the quantity of granite in the source of the Niutitang Formation can be nominal if other processes eliminated the original K_2O/Al_2O_3 from the system.
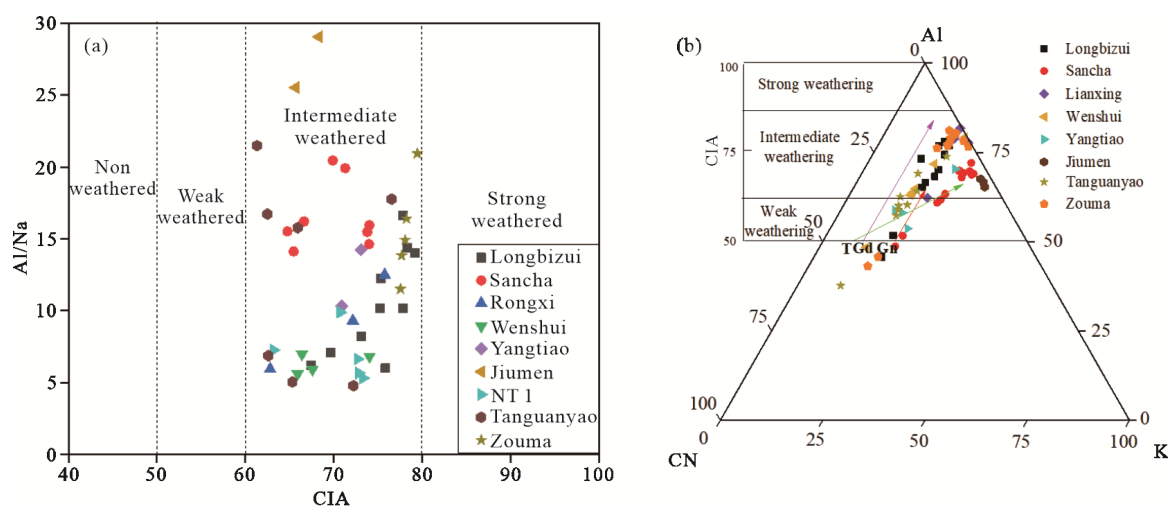

Figure 8. (a) Diagram showing the relationship between the CIA and Al/Na reveals the degree of weathering (modified after Ding et al., 2018). (b) A-CN-K ternary diagram of the Niutitang Formation; T. tonalite; Gn. granodiorite; G. granite. Some data from Jia et al. (2018); Zhou et al. (2017).

These explications are coherent with the interpretation of trace elemental composition.

4.6 Sedimentary Source and Origin of Rare Earth Elements

To determine the source of rocks is a substantial element in determining the paleoenvironmental conditions of that rock. The most viable indicator in identifying the source of a rock is the ratio of SiO_2/Al_2O_3. The studied sections reveal the average value of SiO_2/Al_2O_3 is relatively higher than that of the crust (3.6, Table 2). These higher values indicate the sedimentary supply of silicious matter was not only from a terrestrial source but also from hydrothermal action or biological input. One of the significant indicators for determining the geotectonic environment is the ratio of MnO and TiO_2. Most of the studied samples display lower MnO/TiO_2 (<0.5) ratios, suggesting the sediment supply was from a marginal sea and continental slope (Sugisaki et al., 1982). The Y/Ho ratios can be used to depict the source of sediments, i.e., marine versus terrestrial (Tang et al., 2009; Webb and Kamber, 2000). If the ratio of Y/Ho is 26–28, it designates the terrestrial sedimentary input. On the other hand, the ratio of Y/Ho is 44–72 indicates a marine sedimentary input. In the studied Logbizui and Sacha sections, some samples have high Y/Ho values greater than 44, indicating mixed terrestrial and marine sources. Compared to the other sections, the average value of the Y/Ho ratio from the lowest to the highest in these sections is as follows: Tanguanyao 28.24, Wenshui 28.94, Lianxing 29.52, Zouma 31.12, Ganziping 32.70, Longbizui 34.54, Sancha 36.69, Yangtiao 38.5, Jiumen 41.27, and Rongxi 41.47. Therefore, on a broader scale, it can be suggested the sediment of the Niutitang Formation that formed during the Early Cambrian period was not only contaminated by terrigenous input, but also by marine biological and hydrothermal deposits. It is also suggested there was a transgression phase of sea level during the Early Cambrian period (Awan et al., 2020). Its depocenter was situated towards the southwestern side, i.e., it was deep on the west and shallow at the east. The quantitative amount of (Gd/Yb) is used to differentiate Archean $(Gd/Yb)_n > 2.0$ and the post Archean strata $(Gd/Yb)_n < 2.0$ (Taylor

and McLennan, 1985). In the studied Logbizui and Sacha sections, the average value of $(Gd/Yb)_n$ is 0.93 to 0.75, respectively (Table 3), which indicates the provenance of the Early Cambrian Niutitang Formation was from the post Archean strata. The distribution of rare earth elements also infers the origin of fine-grained sediments (Kasanzu et al., 2008; McLennan et al., 1993). Commonly, rocks with greater LREE/HREE are thought to be associated with felsic sediments, whereas rocks with lower LREE/HREE proportions are thought to be related to mafic rocks (Roddaz et al., 2006; Taylor and McLennan, 1985). Therefore, the nature of the parent rocks can be traced by the distributional pattern of REE. In this context, we utilized the pattern of REEs in the Niutitang Formation to determine its source. In the studied samples, the quantities of LREEs are higher than the HREEs, similar to the general distribution of REEs in limestones or shales (Ketris and Yudovich, 2009; Condie, 1991; Gromet et al., 1984). The minimum mean quantity of ΣLREE is encountered in the Yangtiao Section (33.29 ppm), where the maximum occurs in the Rongxi Section (460 ppm). In the studied Longbizui and Sancha sections, the average value of LREE/HREE is 10.02 and 8.31, respectively, indicating enrichment of LREE, distinguishing a felsic protolith. These average quantities are far higher than the average values of the Rongxi, Lianxing, Wenshui, Yangtiao, and Jiumen sections. Few immobile elements such as Th and La, are indicative of felsic source rocks, whereas Sc is a feature of mafic sources. To determine the provenance of the fine-grained black rocks in the study area, we used a diverse proportion of immobile elements, e. g., Th/Co, Th/Sc, Cr/Th, La/Co, and La/Sc. These elements are vital as they are not affected by sedimentation processes (Nowrouzi et al., 2014; Cullers and Podkovyrov, 2000). The comparison of these elements in the Niutitang Formation and their relative values in oceanic crust, upper, and lower continental crust is presented in Table 5. The value of these ratios is closer to felsic rock sediments compared to sediments from mafic rocks. Therefore, it can be suggested the black rocks in Niutitang Formation are probably of a felsic origin (Table 5). The source and the composition of the specimen can be examined through various geochemical constraints. The
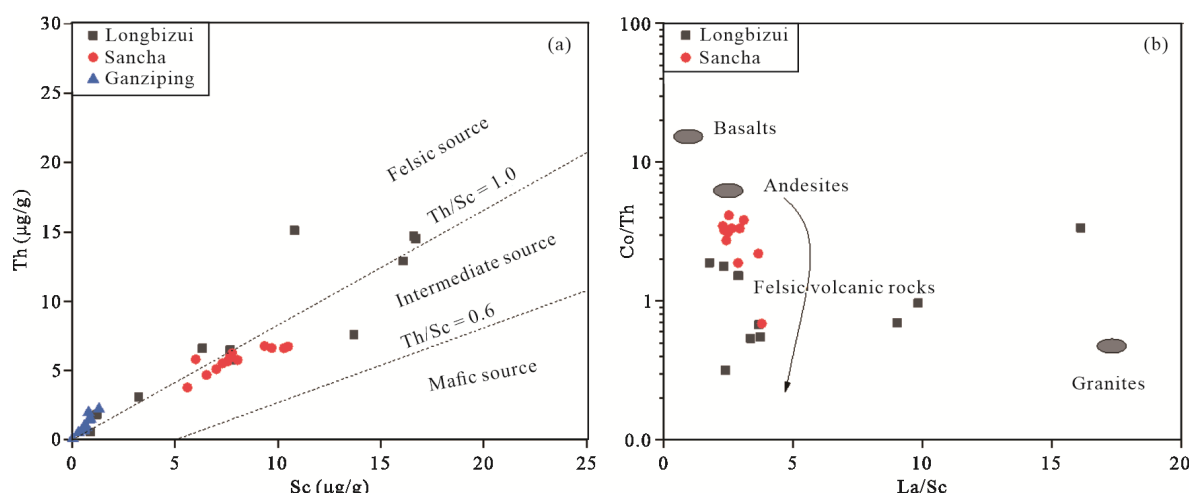

Figure 9. Diagrams displaying the discrimination of compositions and sources. (a) Sc vs. Th; (b) La/Sc vs. Co/Th for the black rocks of Niutitang Formation. Some data from Pan et al. (2004).

Table 5 The ratios of immobile elements in the Niutitang Formation and their average ranges in felsic, mafic, LLC, OC, and UCC rocks to determine the provenance of the rocks

Elements ratio	Range in the present research	LCC[a]	UCC[a]	OC[b]	Range from felsic source[b]	Range from mafic source[b]
Th/Co	0.22–6.68	0.06	0.63	0.01	0.67–19.4	0.04–1.14
Th/Sc	0.55–2.41	0.06	0.79	0.94	0.84–20.5	0.05–0.22
Cr/Th	3.81–336.07	109.5	7.76	-	4.0–15.0	25–500
La/Co	1.03–12.54	0.33	1.76	-	1.80–13.8	0.14–0.38
La/Sc	1.77–16.11	0.31	2.21	0.10	2.5–16.3	0.43–0.76

[a]. LCC and UCC data from McLennan et al. (1993); Taylor and McLennan (1985); [b]. OC and range of felsic and mafic sources are from Cullers and Podkovyrov (2000).

relationship between Th and Sc indicates that the Niutitang Formation black rocks in the studied region were primarily from a felsic or intermediate source (Fig. 9a). Furthermore, most of the specimens in the La/Sc vs. Co/Th crossplot lie in the zone of felsic volcanic rocks (Fig. 9b).

This observational evidence decisively indicates felsic sediments formed the Niutitang Formation. Here we also incorporated ternary diagrams of Co-Th-Zr/10 and Sc-Th-La to depict the tectonic conditions of the Niutitang Formation (Fig. S6). According to the ternary graph of Sc-Th-La (Fig. S6a), most examined specimens lie in the zone of continental island arc settings, while a few are in the region of active and passive continental margins. Similarly, Co-Th-Zr/10 ternary plot (Fig. S6b) shows scattered distribution of the specimens, but a greater number of samples fall within the zone of a continental island arc and in the active continental margin. Hence, in a broader sense, these geochemical constraints suggest the black rock sediments of Niutitang Formation in the study area were from a continental island arc and active continental margin. Cr in deep oceanic or in metalliferous rocks originated from terrigenous detrital particles, which indicate that Cr is associated with other metals like Zr. However, uncertain evidence may suggest a share of Cr is enriched in sediments that were deposited during hydrothermal events in the absence of elemental emigration. The ratio Cr/Zr exhibits a definite affinity with metalliferous and deep oceanic rocks. However, the source region is abruptly dissimilar in hot water metalliferous rocks, and enrichment of Cr is not linked with Zr (Fig. S7a). The sedimentary source and the structural framework for black marine rocks can be distinguished using a ternary graph of Ta-Th-, Hf/3 (Fig. S7b). According to the ternary diagram, a considerable proportion of specimens from the Niutitang Formation lie in Zone I revealing these sediments were associated with a divergent plate boundary. In this study, all the comprehensive analyses based on different ratios and graphs can infer the black rocks of the Niutitang Formation in the area were potentially influenced by deep-seated hydrothermal activities.

4.7   Controlling Factors for the Distribution of REEs

The REEs and Ti and Al elements are thought to be immobile throughout transformation processes (Karadağ et al., 2009; Liaghat et al., 2003). There is a positive association between REEs and Ti and Al elements in the Niutitang Formation black rocks (Figs. S8 and S9). This positive linkage reveals negligi-

ble or weak mobility of REEs and is considered resistant to fractionation through weathering in the various surficial settings. In the black sediments of the Niutitang Formation, coarse grained detrital minerals are few or rare. Therefore it is suggested the occurrence mode of REEs in the Niutitang Formation might be substantially due to adsorption on OM or fine-grain minerals. Al_2O_3 and TiO_2 of the Niutitang Formation display a positive linkage with REEs' individual concentration (Figs. S8 and S9). These positive linkages might reveal clay minerals that might chiefly control the concentration of REEs in the black sediments of the Niutitang Formation. Figure 2 reveals a positive association between various major element oxides (SiO_2, Al_2O_3, Na_2O, MgO, CaO, Fe_2O_3, MnO, K_2O, P_2O_5, and TiO_2) and REEs. Moreover, the significant positive relationship between REEs and Fe_2O_3 content suggests that pyrite could separately control the REEs' concentration. Total organic carbon also exhibits a positive association with the REEs, deciphering the rare earth elements' affinity. Mn and P are the most significant nutrients for plant growth (Chatziapostolou et al., 2006). It is also suggested element P could be chiefly associated with bioproductivity (Awan et al., 2020; Brumsack, 2006; Webb and Kamber, 2000). The REEs in coals are thought to be mainly linked with fine-grain P (Finkelman, 1982). It is also observed in the present research the P_2O_5 and REEs exhibited a positive association that could indicate the REEs in the Niutitang Formation might be associated with the fine-grained phosphates. Moreover, the combinational availability of anoxic settings and higher biological productivities might have created favorable conditions during the Early Cambrian period. The relationship of REEs with certain mobile trace elements (TEs) within the upper continental crust is presented in Fig. S10. Non-clastic sedimentary rocks such as evaporites and limestones, contain a lower proportion of V, Zr, and Ba. These lower quantities are analogous to the mean upper crustal values of shales. In the Niutitang Formation, the value of La vs. V in the majority of the samples is slightly lower than the compositional value in the upper crust. However, the specimens from the Ganziping Section have an unexpectedly higher concentration than upper continental crust, while the Zouma section reaches the limit of the upper crust (Fig. S10a). Similarly, the amount of La vs. Ba is also lower than the limits of the upper continental crust although a couple of them have a higher quantity (Fig. S10b). In contrast, La vs. Zr value in the studied samples has a higher value relative to the upper continental
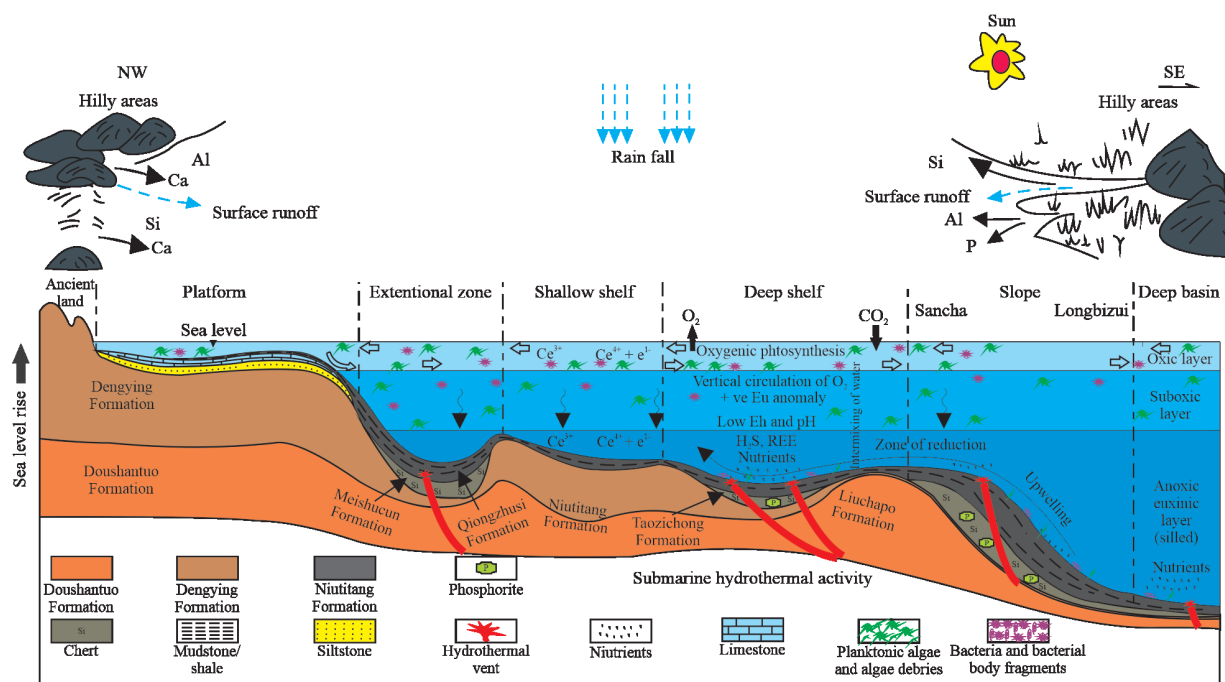
Figure 10. The schematic model of paleoceanography. The model reveals the paleo-oceanic upwelling and mixing of waterbodies elucidating variation in anomalies during the deposition of the Early Cambrian Niutitang Formation.

crust (Fig. S10c) due to the immobile nature of elements during deposition and diagenesis. The lower values of La/V, La/Ba, and the higher quantities of La/Zr relative to the upper continental crust reveal depletion of V, Ba, and enrichment of Zr during deposition of the sediments (McLennan, 2001). Under an extremely low Eh environment, Eu^{3+} reduces to Eu^{2+}. Further, the increase of Eu under severe reducing settings favored substantial mobilization of Eu, which was responsible for the decrease and mobilization of Eu. The higher concentration of organic carbon in these rocks is due to the higher biological productivity and nutrients supply from the deep crust through hydrothermal veins. The diagenesis under alkaline conditions or in extremely reducing settings is beneficial for the reduction of Eu3+, although its reduction is very rare in other conditions. The occurrence of pyrite and organic matter in these sediments is a sign of anoxic settings, whereas the presence of carbonate (dolomite and calcite) minerals indicate alkaline environments in the basin during deposition. The positive Eu anomalies of the studied specimens indicate the Niutitang Formation in the study area was highly affected with deep water hydrothermal fluids. These anomalies (Eu and Ce), along with original seawater features, favor deposition of these black sediments by intermixing oxic and anoxic seawater through upwelling phenomena during the Early Cambrian period. Due to this upwelling mechanism, deep-seated anoxic rich Ce^{3+} and OM moved towards the upper oxic zone. In the upper region, it reduced Ce through oxidization of Ce^{3+}-Ce^{4+}. Ce depleted by intermixing, and the Eu anomaly, together with organically enriched water that migrated over the shallower part of the marine basin, show that these currents also deposited the black rocks (Fig. 10).

5 CONCLUSIONS

This research primarily discusses the geochemical charac-

terization of organic-rich black rocks of the Early Cambrian Niutitang Formation from the Xiangxi area to evaluate its paleoenvironmental conditions during the Early Cambrian period. Conclusive outcomes of this research are as follows.

(1) The total organic carbon content in the platform region is extremely low, indicating a poor potential to produce hydrocarbons. In contrast, significantly higher TOC quantities are observed in the deep shelf and slope sediments, indicating a significantly higher potential to produce hydrocarbons.

(2) Black rock sediments with enrichment of rare earth elements in unexpectedly low quantities are observed in Yangtiao and Rongxi areas. The enrichment of REEs, positive Eu anomaly, negative Ce anomaly, and a moderate Y/Ho are the clues for a hybrid mechanism associated with hydrothermal action and the terrigenous input.

(3) The values of the chemical index of weathering, chemical index of alteration, and index for compositional variability reveal these black rock sediments might be from moderate weathered sources. Additionally, the sediments of the Niutitang Formation in the study area were sourced from continental island arcs and active continental margins. The immobile elements such as Th/Co, Th/Sc, Cr/Th, La/Co, and La/Sc that are not affected by sedimentation processes, suggest the Niutitang Formation is closer to the felsic rock sediments. Moreover, the susceptible trace elements V, Ni, Cu and negative Ce anomaly indicate the Niutitang Formation was deposited in oxygen-depleted/anoxic conditions and deeper water levels in weak hydrodynamic conditions, which were beneficial for the preservation and enrichment of organic matters.

(4) The main controlling factors for the distribution of rare earth elements in these black rocks of the Niutitang Formation are pH, terrigenous input, source rock composition, tectonism, upwelling mechanism, and hydrothermal activities.

Conflict of Interest

The authors declare that they have no conflict of interest.

REFERENCES CITED

Algeo, T. J., 2004. Can Marine Anoxic Events Draw down the Trace Element Inventory of Seawater? *Geology*, 32(12): 1057–1060. https://doi.org/10.1130/g20896.1

Algeo, T. J., Maynard, J. B., 2008. Trace-Metal Covariation as a Guide to Water-Mass Conditions in Ancient Anoxic Marine Environments. *Geosphere*, 4(5): 872–887. https://doi.org/10.1130/ges00174.1

Allegre, C.-J., Michard, G., 1974. Introduction to Geochemistry. D. Reidel Publishing Company, Dordrecht. 10. https://doi.org/10.1007/978-94-010-2261-3

Amthor, J. E., Grotzinger, J. P., Schröder, S., et al., 2003. Extinction of Cloudina and Namacalathus at the Precambrian-Cambrian Boundary in Oman. *Geology*, 31(5): 431–434. https://doi.org/10.1130/0091-7613(2003)0310431:eocana>2.0.co;2

Arthur, M. A., Sageman, B. B., 2005. Sea-Level Control on Source-Rock Development: Perspectives from the Holocene Black Sea, the Mid-Cretaceous Western Interior Basin of North America, and the Late Devonian Appalachian Basin. In: Harris, N. B., ed., The Deposition of Organic-Carbon-Rich Sediments: Models, Mechanisms, and Consequences. SEPM (Society for Sedimentary Geology). 35–59. https://doi.org/10.2110/pec.05.82.0035

Awan, R. S., Liu, C. L., Aadil, N., et al., 2021a. Organic Geochemical Evaluation of Cretaceous Talhar Shale for Shale Oil and Gas Potential from Lower Indus Basin, Pakistan. *Journal of Petroleum Science and Engineering*, 200: 108404. https://doi.org/10.1016/j.petrol.2021.108404

Awan, R. S., Liu, C. L., Yang, S. F., et al., 2021b. The Occurrence of Vanadium in Nature: Its Biogeochemical Cycling and Relationship with Organic Matter—A Case Study of the Early Cambrian Black Rocks of the Niutitang Formation, Western Hunan, China. *Acta Geochimica*, 40(6): 973–997. https://doi.org/10.1007/s11631-021-00482-2

Awan, R. S., Liu, C. L., Gong, H. W., et al., 2020. Paleo-Sedimentary Environment in Relation to Enrichment of Organic Matter of Early Cambrian Black Rocks of Niutitang Formation from Xiangxi Area China. *Marine and Petroleum Geology*, 112: 104057. https://doi.org/10.1016/j.marpetgeo.2019.104057

Bau, M., Dulski, P., 1996. Distribution of Yttrium and Rare-Earth Elements in the Penge and Kuruman Iron-Formations, Transvaal Supergroup, South Africa. *Precambrian Research*, 79(1/2): 37–55. https://doi.org/10.1016/0301-9268(95)00087-9

Bock, B., McLennan, S. M., Hanson, G. N., 1998. Geochemistry and Provenance of the Middle Ordovician Austin Glen Member (Normanskill Formation) and the Taconian Orogeny in New England. *Sedimentology*, 45(4): 635–655. https://doi.org/10.1046/j.1365-3091.1998.00168.x

Brumsack, H.-J., 2006. The Trace Metal Content of Recent Organic Carbon-Rich Sediments: Implications for Cretaceous Black Shale Formation. *Palaeogeography, Palaeoclimatology, Palaeoecology*, 232(2/3/4): 344–361. https://doi.org/10.1016/j.palaeo.2005.05.011

Brumsack, H. J., 1989. Geochemistry of Recent TOC-Rich Sediments from the Gulf of California and the Black Sea. *Geologische Rundschau*, 78(3): 851–882. https://doi.org/10.1007/bf01829327

Cai, L. G., Liu, H. F., 1996. Evolution and Structural Styles of the Sichuan Foreland Basin: In: Global Tectonic Zones Supercontinent Formation and Disposal: Proceedings of the 30th International Geological Congress, Aug. 4–14, 1996, Beijing. 87

Chatziapostolou, A., Kalaitzidis, S., Papazisimou, S., et al., 2006. Mode of Occurrence of Trace Elements in the Pellana Lignite (SE Peloponnese, Greece). *International Journal of Coal Geology*, 65(1/2): 3–16. https://doi.org/10.1016/j.coal.2005.04.005

Choi, J. H., Hariya, Y., 1992. Geochemistry and Depositional Environment of Mn Oxide Deposits in the Tokoro Belt, Northeastern Hokkaido, Japan. *Economic Geology*, 87(5): 1265–1274. https://doi.org/10.2113/gsecongeo.87.5.1265

Clark, S. H. B., Poole, F. G., Wang, Z. C., 2004. Comparison of some Sediment-Hosted, Stratiform Barite Deposits in China, the United States, and India. *Ore Geology Reviews*, 24(1/2): 85–101. https://doi.org/10.1016/j.oregeorev.2003.08.009

Condie, K. C., 1991. Another Look at Rare Earth Elements in Shales. *Geochimica et Cosmochimica Acta*, 55(9): 2527–2531. https://doi.org/10.1016/0016-7037(91)90370-k

Condie, K. C., 1993. Chemical Composition and Evolution of the Upper Continental Crust: Contrasting Results from Surface Samples and Shales. *Chemical Geology*, 104(1/2/3/4): 1–37. https://doi.org/10.1016/0009-2541(93)90140-e

Cox, R., Lowe, D. R., 1995. Controls on Sediment Composition on a Regional Scale: A Conceptual Review. *Journal of Sedimentary Research*, 65(1a): 1–12. https://doi.org/10.1306/d4268009-2b26-11d7-8648000102c1865d

Cullers, R. L., Podkovyrov, V. N., 2000. Geochemistry of the Mesoproterozoic Lakhanda Shales in Southeastern Yakutia, Russia: Implications for Mineralogical and Provenance Control, and Recycling. *Precambrian Research*, 104(1/2): 77–93. https://doi.org/10.1016/s0301-9268(00)00090-5

Dai, S. F., Li, D., Chou, C. L., et al., 2008. Mineralogy and Geochemistry of Boehmite-Rich Coals: New Insights from the Haerwusu Surface Mine, Jungar Coalfield, Inner Mongolia, China. *International Journal of Coal Geology*, 74(3/4): 185–202. https://doi.org/10.1016/j.coal.2008.01.001

Ding, J. H., Zhang, J. C., Tang, X., et al., 2018. Elemental Geochemical Evidence for Depositional Conditions and Organic Matter Enrichment of Black Rock Series Strata in an Inter-Platform Basin: The Lower Carboniferous Datang Formation, Southern Guizhou, Southwest China. *Minerals*, 8(11): 509. https://doi.org/10.3390/min8110509

Dubinin, A. V., 2004. Geochemistry of Rare Earth Elements in the Ocean. *Lithology and Mineral Resources*, 39(4): 289–307. https://doi.org/10.1023/b:limi.0000033816.14825.a2

Dulski, P., 1994. Interferences of Oxide, Hydroxide and Chloride Analyte Species in the Determination of Rare Earth Elements in Geological Samples by Inductively Coupled Plasma-Mass Spectrometry. *Fresenius Journal of Analytical Chemistry*, 350(4): 194–203. https://doi.org/10.1007/bf00322470

Elderfield, H., Greaves, M. J., 1982. The Rare Earth Elements in Seawater.

Nature, 296(5854): 214–219. https://doi.org/10.1038/296214a0

Fedo, C. M., Wayne Nesbitt, H., Young, G. M., 1995. Unraveling the Effects of Potassium Metasomatism in Sedimentary Rocks and Paleosols, with Implications for Paleoweathering Conditions and Provenance. *Geology*, 23(10): 921–924. https://doi.org/10.1130/0091-7613(1995)0230921:uteopm>2.3.co;2

Fedo, C. M., Young, G. M., Nesbitt, H. W., 1997. Paleoclimatic Control on the Composition of the Paleoproterozoic Serpent Formation, Huronian Supergroup, Canada: A Greenhouse to Icehouse Transition. *Precambrian Research*, 86(3/4): 201–223. https://doi. org/10.1016/s0301-9268(97)00049-1

Finkelman, R. B., 1982. The Origin, Occurrence, and Distribution of the Inorganic Constituents in Low-Rank Coals. In: Proceedings of the Basic Coal Science Workshop. US Department of Energy, Houston, TX. 69–90

Gao, P., He, Z. L., Li, S. J., et al., 2018. Volcanic and Hydrothermal Activities Recorded in Phosphate Nodules from the Lower Cambrian Niutitang Formation Black Shales in South China. *Palaeogeography, Palaeoclimatology, Palaeoecology*, 505: 381–397. https://doi. org/10.1016/j.palaeo.2018.06.019

German, C. R., Elderfield, H., 1990. Application of the Ce Anomaly as a Paleoredox Indicator: The Ground Rules. *Paleoceanography*, 5(5): 823–833. https://doi.org/10.1029/pa005i005p00823

Grandjean, P., Cappetta, H., Albarède, F., 1988. The Ree and ε_{Nd} of 40–70 Ma Old Fish Debris from the West-African Platform. *Geophysical Research Letters*, 15(4): 389–392. https://doi.org/10.1029/gl015i004p00389

Gromet, L. P., Haskin, L. A., Korotev, R. L., et al., 1984. The "North American Shale Composite": Its Compilation, Major and Trace Element Characteristics. *Geochimica et Cosmochimica Acta*, 48(12): 2469–2482. https://doi.org/10.1016/0016-7037(84)90298-9

Guo, Q. J., Shields, G. A., Liu, C. Q., et al., 2007. Trace Element Chemostratigraphy of Two Ediacaran-Cambrian Successions in South China: Implications for Organosedimentary Metal Enrichment and Silicification in the Early Cambrian. *Palaeogeography, Palaeoclimatology, Palaeoecology*, 254(1/2): 194–216. https://doi.org/10.1016/j.palaeo.2007.03.016

Hall, P. A., 2012. Elemental, Isotopic and Molecular Signatures of Early Cambrian Marine Sediments and a Phantom Petroleum System in South Australia: [Dissertation]. Geology and Geophysics School of Earth and Environmental, Science Faculty of Science, University of Adelaide, Adelaide

Han, T., Zhu, X. Q., Li, K., et al., 2015. Metal Sources for the Polymetallic Ni-Mo-PGE Mineralization in the Black Shales of the Lower Cambrian Niutitang Formation, South China. *Ore Geology Reviews*, 67: 158–169. https://doi.org/10.1016/j.oregeorev.2014.11.020

Haskin, L. A., Wildeman, T. R., Haskin, M. A., 1968. An Accurate Procedure for the Determination of the Rare Earths by Neutron Activation. *Journal of Radioanalytical Chemistry*, 1(4): 337–348. https://doi.org/10.1007/bf02513689

Holser, W. T., 1997. Evaluation of the Application of Rare-Earth Elements to Paleoceanography. *Palaeogeography, Palaeoclimatology, Palaeoecology*, 132(1/2/3/4): 309–323. https://doi. org/10.1016/s0031-0182(97)00069-2

Jia, Z. B., Hou, D. J., Sun, D. Q., et al., 2018. Geochemical Characteristics of Source Rocks in the Lower Cambrian Niutitang Formation in Guizhou Province, China. *Journal of Natural Gas Geoscience*, 3(5): 263–272. https://doi.org/10.1016/j.jnggs.2018.11.005

Jiang, G. Q., Shi, X. Y., Zhang, S. H., et al., 2011. Stratigraphy and Paleogeography of the Ediacaran Doushantuo Formation (ca. 635–551

Ma) in South China. *Gondwana Research*, 19(4): 831–849. https://doi. org/10.1016/j.gr.2011.01.006

Jiang, S. Y., Pi, D. H., Heubeck, C., et al., 2009. Early Cambrian Ocean Anoxia in South China. *Nature*, 459: E5–E6. https://doi.org/10.1038/nature08048

Jiang, Z. Z., Sun, Z. L., Liu, Z. Q., et al., 2019. Rare-Earth Element Geochemistry Reveals the Provenance of Sediments on the Southwestern Margin of the Challenger Deep. *Journal of Oceanology and Limnology*, 37(3): 998–1009. https://doi.org/10.1007/s00343-019-8046-8

Kamber, B. S., Webb, G. E., 2001. The Geochemistry of Late Archaean Microbial Carbonate: Implications for Ocean Chemistry and Continental Erosion History. *Geochimica et Cosmochimica Acta*, 65(15): 2509–2525. https://doi.org/10.1016/s0016-7037(01)00613-5

Karadağ, M. M., Küpeli, Ş., Arýk, F., et al., 2009. Rare Earth Element (REE) Geochemistry and Genetic Implications of the Mortaş Bauxite Deposit (Seydişehir/Konya-Southern Turkey). *Geochemistry*, 69(2): 143–159. https://doi.org/10.1016/j.chemer.2008.04.005

Kasanzu, C., Maboko, M. A. H., Manya, S., 2008. Geochemistry of Fine-Grained Clastic Sedimentary Rocks of the Neoproterozoic Ikorongo Group, NE Tanzania: Implications for Provenance and Source Rock Weathering. *Precambrian Research*, 164(3/4): 201–213. https://doi.org/10.1016/j.precamres.2008.04.007

Katz, B. J., 2005. Controlling Factors on Source Rock Development—A Review of Productivity, Preservation, and Sedimentation Rate. Deposition of Organic-Carbon-Rich Sediments: Models. *SEPM (Society for Sedimentary Geology)*, 82: 7–16. https://doi.org/10.2110/pec.05.82.0007

Ketris, M. P., Yudovich, Y. E., 2009. Estimations of Clarkes for Carbonaceous Biolithes: World Averages for Trace Element Contents in Black Shales and Coals. *International Journal of Coal Geology*, 78(2): 135–148. https://doi.org/10.1016/j.coal.2009.01.002

Kidder, D. L., Krishnaswamy, R., Mapes, R. H., 2003. Elemental Mobility in Phosphatic Shales during Concretion Growth and Implications for Provenance Analysis. *Chemical Geology*, 198(3/4): 335–353. https://doi.org/10.1016/s0009-2541(03)00036-6

Lehmann, B., Nägler, T. F., Holland, H. D., et al., 2007. Highly Metalliferous Carbonaceous Shale and Early Cambrian Seawater. *Geology*, 35(5): 403–406. https://doi.org/10.1130/g23543a.1

Li, C., Love, G. D., Lyons, T. W., et al., 2010. A Stratified Redox Model for the Ediacaran Ocean. *Science*, 328(5974): 80–83. https://doi. org/10.1126/science.1182369

Li, D. L., Li, R. X., Tan, C. Q., et al., 2019. Origin of Silica, Paleoenvironment, and Organic Matter Enrichment in the Lower Paleozoic Niutitang and Longmaxi Formations of the Northwestern Upper Yangtze Plate: Significance for Hydrocarbon Exploration. *Marine and Petroleum Geology*, 103: 404–421. https://doi.org/10.1016/j.marpetgeo.2019.02.025

Li, J., Yu, B. S., Guo, F., 2013. Depositional Setting and Tectonic Background Analysis on Lower Cambrian Black Shales in the North of Guizhou Province. *Acta Sedimentologica Sinica*, 31(1): 20–31. https://doi.org/10.14027/j.cnki.cjxb.2013.01.012 (in Chinese English Abstract)

Liaghat, S., Hosseini, M., Zarasvandi, A., 2003. Determination of the Origin and Mass Change Geochemistry during Bauxitization Process at the Hangam Deposit, SW Iran. *Geochemical Journal*, 37(5): 627–637. https://doi.org/10.2343/geochemj.37.627

Liu, B. J., Xu, X. S., 1994. Atlas of Paleogeography and Lithofacies of South China: (Sinian-Trias). Science Press, Beijing. 1–188 (in Chinese)

Liu, J., Yao, Y. B., Elsworth, D., et al., 2016. Sedimentary Characteristics of the Lower Cambrian Niutitang Shale in the Southeast Margin of Sichuan Basin, China. *Journal of Natural Gas Science and Engineering*, 36: 1140–1150. https://doi.org/10.1016/j.jngse.2016.03.085

Liu, Z. H., Zhuang, X. G., Teng, G. E., et al., 2015. The Lower Cambrian Niutitang Formation at Yangtiao (Guizhou, Sw China): Organic Matter Enrichment, Source Rock Potential, and Hydrothermal Influences. *Journal of Petroleum Geology*, 38(4): 411–432. https://doi.org/10.1111/jpg.12619

Luo, C., 2014. Geological Characteristics of Gas Shale in the Lower Cambrian Niutitang Formation of the Upper Yangtze Platform. Chengdu University of Technology, Chengdu. 115–132 (in Chinese with English Abstract)

Loucks, R. G., Ruppel, S. C., 2007. Mississippian Barnett Shale: Lithofacies and Depositional Setting of a Deep-Water Shale-Gas Succession in the Fort Worth Basin, Texas. *AAPG Bulletin*, 91(4): 579–601. https://doi.org/10.1306/11020606059

Ma, K., Hu, S. Y., Wang, T. S., et al., 2017. Sedimentary Environments and Mechanisms of Organic Matter Enrichment in the Mesoproterozoic Hongshuizhuang Formation of Northern China. *Palaeogeography, Palaeoclimatology, Palaeoecology*, 475: 176–187. https://doi.org/10.1016/j.palaeo.2017.02.038

Marchig, V., Gundlach, H., Möller, P., et al., 1982. Some Geochemical Indicators for Discrimination between Diagenetic and Hydrothermal Metalliferous Sediments. *Marine Geology*, 50(3): 241–256. https://doi.org/10.1016/0025-3227(82)90141-4

McLennan, S. M., 2001. Relationships between the Trace Element Composition of Sedimentary Rocks and Upper Continental Crust. *Geochemistry, Geophysics, Geosystems*, 2(4): 1021–1041. https://doi.org/10.1029/2000gc000109

McLennan, S. M., Hemming, S., McDaniel, D. K., et al., 1993. Geochemical Approaches to Sedimentation, Provenance, and Tectonics. Processes Controlling the Composition of Clastic Sediments. Geological Society of America. 21–40. https://doi.org/10.1130/spe284-p21

Moffett, J. W., 1990. Microbially Mediated Cerium Oxidation in Sea Water. *Nature*, 345(6274): 421–423. https://doi.org/10.1038/345421a0

Morad, S., Felitsyn, S., 2001. Identification of Primary Ce-Anomaly Signatures in Fossil Biogenic Apatite: Implication for the Cambrian Oceanic Anoxia and Phosphogenesis. *Sedimentary Geology*, 143(3/4): 259–264. https://doi.org/10.1016/s0037-0738(01)00093-8

Munksgaard, N. C., Lim, K., Parry, D. L., 2003. Rare Earth Elements as Provenance Indicators in North Australian Estuarine and Coastal Marine Sediments. *Estuarine, Coastal and Shelf Science*, 57(3): 399–409. https://doi.org/10.1016/s0272-7714(02)00368-2

Nesbitt, H. W., Young, G. M., 1982. Early Proterozoic Climates and Plate Motions Inferred from Major Element Chemistry of Lutites. *Nature*, 299(5885): 715–717. https://doi.org/10.1038/299715a0

Nowrouzi, Z., Moussavi-Harami, R., Mahboubi, A., et al., 2014. Petrography and Geochemistry of Silurian Niur Sandstones, Derenjal Mountains, East Central Iran: Implications for Tectonic Setting, Provenance and Weathering. *Arabian Journal of Geosciences*, 7(7): 2793–2813. https://doi.org/10.1007/s12517-013-0912-7

Och, L. M., Shields-Zhou, G. A., Poulton, S. W., et al., 2013. Redox Changes in Early Cambrian Black Shales at Xiaotan Section, Yunnan Province, South China. *Precambrian Research*, 225: 166–189. https://doi.org/10.1016/j.precamres.2011.10.005

Ogihara, S., 1999. Geochemical Characteristics of Phosphorite and Carbonate Nodules from the Miocene Funakawa Formation, Western Margin of the Yokote Basin, Northeast Japan. *Sedimentary Geology*, 125(1/2): 69–82. https://doi.org/10.1016/s0037-0738(98)00136-5

Orberger, B., Vymazalova, A., Wagner, C., et al., 2007. Biogenic Origin of Intergrown Mo-Sulphide- and Carbonaceous Matter in Lower Cambrian Black Shales (Zunyi Formation, Southern China). *Chemical Geology*, 238(3/4): 213–231. https://doi.org/10.1016/j.chemgeo.2006.11.010

Pan, J. Y., Ma, D. S., Cao, S. L., 2004. Trace Element Geochemistry of the Lower Cambrian Black Rock Series from Northwestern Hunan, South China. *Progress in Natural Science*, 14(1): 64–70. https://doi.org/10.1080/10020070412331343161

Peters, K., Cassa, M. R., 1994. Applied Source Rock Geochemistry: Chapter 5: Part II. In: Magoon, L. B., Dow, W. G., eds., The Petroleum System. From Source to Trap. American Association of Petroleum Geologists, Tulsa. 93–120

Pi, D. H., Liu, C. Q., Shields-Zhou, G. A., et al., 2013. Trace and Rare Earth Element Geochemistry of Black Shale and Kerogen in the Early Cambrian Niutitang Formation in Guizhou Province, South China: Constraints for Redox Environments and Origin of Metal Enrichments. *Precambrian Research*, 225: 218–229. https://doi.org/10.1016/j.precamres.2011.07.004

Plank, T., Langmuir, C. H., 1998. The Chemical Composition of Subducting Sediment and Its Consequences for the Crust and Mantle. *Chemical Geology*, 145(3/4): 325–394. https://doi.org/10.1016/s0009-2541(97)00150-2

Roddaz, M., Viers, J., Brusset, S., et al., 2006. Controls on Weathering and Provenance in the Amazonian Foreland Basin: Insights from Major and Trace Element Geochemistry of Neogene Amazonian Sediments. *Chemical Geology*, 226(1/2): 31–65. https://doi.org/10.1016/j.chemgeo.2005.08.010

Rona, P. A., 1978. Criteria for Recognition of Hydrothermal Mineral Deposits in Oceanic Crust. *Economic Geology*, 73(2): 135–160. https://doi.org/10.2113/gsecongeo.73.2.135

Rudnick, R. L., Gao, S., 2003. Composition of the Continental Crust. Treatise on Geochemistry. Elsevier, Amsterdam. 1–64. https://doi.org/10.1016/b0-08-043751-6/03016-4

Schijf, J., de Baar, H. J. W., Wijbrans, J. R., et al., 1991. Dissolved Rare Earth Elements in the Black Sea. *Deep Sea Research Part A Oceanographic Research Papers*, 38: S805–S823. https://doi.org/10.1016/s0198-0149(10)80010-x

Sharma, A., Rajamani, V., 2000a. Weathering of Gneissic Rocks in the Upper Reaches of Cauvery River, South India: Implications to Neotectonics of the Region. *Chemical Geology*, 166(3/4): 203–223. https://doi.org/10.1016/s0009-2541(99)00222-3

Sharma, A., Rajamani, V., 2000b. Major Element, REE, and other Trace Element Behavior in Amphibolite Weathering under Semiarid Conditions in Southern India. *The Journal of Geology*, 108(4): 487–496. https://doi.org/10.1086/314409

Shen, Y. N., Schidlowski, M., Chu, X. L., 2000. Biogeochemical Approach to Understanding Phosphogenic Events of the Terminal Proterozoic to Cambrian. *Palaeogeography, Palaeoclimatology, Palaeoecology*, 158(1/2): 99–108. https://doi.org/10.1016/s0031-0182(00)00033-x

Shields, G., Stille, P., 2001. Diagenetic Constraints on the Use of Cerium Anomalies as Palaeoseawater Redox Proxies: An Isotopic and REE Study of Cambrian Phosphorites. *Chemical Geology*, 175(1/2): 29–48. https://doi.org/10.1016/s0009-2541(00)00362-4

Sholkovitz, E. R., Landing, W. M., Lewis, B. L., 1994. Ocean Particle Chemistry: The Fractionation of Rare Earth Elements between Suspended Particles and Seawater. *Geochimica et Cosmochimica Acta*,

58(6): 1567–1579. https://doi.org/10.1016/0016-7037(94)90559-2

Singh, P., 2009. Major, Trace and REE Geochemistry of the Ganga River Sediments: Influence of Provenance and Sedimentary Processes. *Chemical Geology*, 266(3/4): 242 – 255. https://doi. org/10.1016/j. chemgeo.2009.06.013

Singh, P., Rajamani, V., 2001. REE Geochemistry of Recent Clastic Sediments from the Kaveri Floodplains, Southern India: Implication to Source Area Weathering and Sedimentary Processes. *Geochimica et Cosmochimica Acta*, 65(18): 3093 – 3108. https://doi. org/10.1016/ s0016-7037(01)00636-6

Steiner, M., Li, G. X., Qian, Y., et al., 2007. Neoproterozoic to Early Cambrian Small Shelly Fossil Assemblages and a Revised Biostratigraphic Correlation of the Yangtze Platform (China). *Palaeogeography*, *Palaeoclimatology*, *Palaeoecology*, 254(1/2): 67–99. https://doi.org/10.1016/j.palaeo.2007.03.046

Steiner, M., Wallis, E., Erdtmann, B. D., et al., 2001. Submarine-Hydrothermal Exhalative Ore Layers in Black Shales from South China and Associated Fossils—Insights into a Lower Cambrian Facies and Bio-Evolution. *Palaeogeography*, *Palaeoclimatology*, *Palaeoecology*, 169(3/4): 165–191. https://doi.org/10.1016/s0031-0182(01)00208-5

Sugisaki, R., Yamamoto, K., Adachi, M., 1982. Triassic Bedded Cherts in Central Japan are not Pelagic. *Nature*, 298(5875): 644–647. https://doi. org/10.1038/298644a0

Tang, H. S., Chen, Y. J., Wu, G., et al., 2009. Rare Earth Element Geochemistry of Carbonates of Dashiqiao Formation, Liaohe Group, Eastern Liaoning Province: Implications for Lomagundi Event. *Acta Petrologica Sinica*, 25(11): 3075–3093 (in Chinese with English Abstract)

Tang, X. L., Jiang, Z. X., Li, Z., et al., 2017. Factors Controlling Organic Matter Enrichment in the Lower Cambrian Niutitang Formation Shale on the Eastern Shelf Margin of the Yangtze Block, China. *Interpretation*, 5(3): T399–T410. https://doi.org/10.1190/int-2017-0008.1

Tang, X., Zhang, J. C., Liu, Y., et al., 2018. Geochemistry of Organic Matter and Elements of Black Shale during Weathering in Northern Guizhou, Southwestern China: Their Mobilization and Inter-Connection. *Geochemistry*, 78(1): 140–151. https://doi.org/10.1016/j.chemer.2017.08.002

Taylor, S. R., McLennan, S. M., 1985. The Continental Crust: Its Composition and Evolution. Blackwell Scientific Publications, Palo Alto. 312

Tian, X. L., Luo, K. L., 2017. Selenium, Arsenic and Molybdenum Variation and Bio-Radiation in the Ediacaran-Cambrian Interval. *Precambrian Research*, 292: 378 – 385. https://doi. org/10.1016/j. precamres.2017.02.007

Tribovillard, N., Algeo, T. J., Lyons, T., et al., 2006. Trace Metals as Paleoredox and Paleoproductivity Proxies: An Update. *Chemical Geology*, 232(1/2): 12–32. https://doi.org/10.1016/j.chemgeo.2006.02.012

Tuo, J. C., Wu, C. J., Zhang, M. F., 2016. Organic Matter Properties and Shale Gas Potential of Paleozoic Shales in Sichuan Basin, China. *Journal of Natural Gas Science and Engineering*, 28: 434–446. https://doi.org/10.1016/j.jngse.2015.12.003

Uysal, I. T., Zhao, J. X., Golding, S. D., et al., 2007. Sm-Nd Dating and Rare-Earth Element Tracing of Calcite: Implications for Fluid-Flow Events in the Bowen Basin, Australia. *Chemical Geology*, 238(1/2): 63–71. https://doi.org/10.1016/j.chemgeo.2006.10.014

Valkovic, V., 1983. Trace Elements in Coal. Florida CRC Press Inc., Coca Raton. Vol. 1. 210

Wang, J. G., Chen, D. Z., Wang, Q. C., et al., 2007. Platform Evolution and Marine Source Rock Deposition during the Terminal Sinian to Early Cambrian in the Middle Yangtze Region. *Acta Geologica Sinica*, 81(8): 1102–1109, 1162 (in Chinese with English Abstract)

Wang, X. Q., Shi, X. Y., Jiang, G. Q., et al., 2012. New U-Pb Age from the Basal Niutitang Formation in South China: Implications for Diachronous Development and Condensation of Stratigraphic Units across the Yangtze Platform at the Ediacaran-Cambrian Transition. *Journal of Asian Earth Sciences*, 48: 1 – 8. https://doi. org/10.1016/j. jseaes.2011.12.023

Webb, G. E., Kamber, B. S., 2000. Rare Earth Elements in Holocene Reefal Microbialites: A New Shallow Seawater Proxy. *Geochimica et Cosmochimica Acta*, 64(9): 1557–1565. https://doi.org/10.1016/s0016-7037(99)00400-7

Weber, B., Steiner, M., Zhu, M. Y., 2007. Precambrian-Cambrian Trace Fossils from the Yangtze Platform (South China) and the Early Evolution of Bilaterian Lifestyles. *Palaeogeography*, *Palaeoclimatology*, *Palaeoecology*, 254(1/2): 328 – 349. https://doi. org/10.1016/j. palaeo. 2007. 03.021

Wilde, P., Quinby-Hunt, M. S., Erdtmann, B. D., 1996. The Whole-Rock Cerium Anomaly: A Potential Indicator of Eustatic Sea-Level Changes in Shales of the Anoxic Facies. *Sedimentary Geology*, 101(1/2): 43–53. https://doi.org/10.1016/0037-0738(95)00020-8

Wille, M., Nägler, T. F., Lehmann, B., et al., 2008. Hydrogen Sulphide Release to Surface Waters at the Precambrian/Cambrian Boundary. *Nature*, 453(7196): 767–769. https://doi.org/10.1038/nature07072

Wu, C. J., Zhang, L. F., Zhang, T. W., et al., 2020. Reconstruction of Paleoceanic Redox Conditions of the Lower Cambrian Niutitang Shales in Northern Guizhou, Upper Yangtze Region. *Palaeogeography*, *Palaeoclimatology*, *Palaeoecology*, 538: 109457. https://doi. org/10.1016/j. palaeo.019.109457

Wu, C. J., Tuo, J. C., Zhang, M. F., et al., 2016. Sedimentary and Residual Gas Geochemical Characteristics of the Lower Cambrian Organic-Rich Shales in Southeastern Chongqing, China. *Marine and Petroleum Geology*, 75: 140–150. https://doi.org/10.1016/j.marpetgeo.2016.04.013

Xu, L. G., Lehmann, B., Mao, J. W., et al., 2011. Re-Os Age of Polymetallic Ni-Mo-PGE-Au Mineralization in Early Cambrian Black Shales of South China: A Reassessment. *Economic Geology*, 106(3): 511 – 522. https://doi.org/10.2113/econgeo.106.3.511

Xu, L. G., Lehmann, B., Mao, J. W., et al., 2012. Mo Isotope and Trace Element Patterns of Lower Cambrian Black Shales in South China: Multi-Proxy Constraints on the Paleoenvironment. *Chemical Geology*, 318/319: 45–59. https://doi.org/10.1016/j.chemgeo.2012.05.016

Yang, B. Y., Hu, B., Bao, Z. Y., et al., 2011. REE Geochemical Characteristics and Depositional Environment of the Black Shale-Hosted Baiguoyuan Ag-V Deposit in Xingshan, Hubei Province, China. *Journal of Rare Earths*, 29(5): 499–506. https://doi.org/10.1016/s1002-0721(10)60488-7

Yang, S. Y., Jung, H. S., Choi, M. S., et al., 2002. The Rare Earth Element Compositions of the Changjiang (Yangtze) and Huanghe (Yellow) River Sediments. *Earth and Planetary Science Letters*, 201(2): 407–419. https://doi.org/10.1016/s0012-821x(02)00715-x

Yeasmin, R., Chen, D. Z., Fu, Y., et al., 2017. Climatic-Oceanic Forcing on the Organic Accumulation across the Shelf during the Early Cambrian (Age 2 through 3) in the Mid-Upper Yangtze Block, NE Guizhou, South China. *Journal of Asian Earth Sciences*, 134: 365–386. https://doi.org/10.1016/j.jseaes.2016.08.019

Zhang, K., Song, Y., Jiang, S., et al., 2019. Mechanism Analysis of Organic Matter Enrichment in Different Sedimentary Backgrounds: a Case Study of the Lower Cambrian and the Upper Ordovician-Lower Silurian, in Yangtze Region. *Marine and Petroleum Geology*, 99: 488–497. https://doi.org/10.1016/j.marpetgeo.2018.10.044

Zhang, Y. Y., He, Z. L., Jiang, S., et al., 2018. Controls on the Organic Carbon Content of the Lower Cambrian Black Shale in the Southeastern Margin of Upper Yangtze. *Petroleum Science*, 15(4): 709–721. https://doi.org/10.1007/s12182-018-0262-x

Zhou, L., Kang, Z. H., Wang, Z. X., et al., 2017. Sedimentary Geochemical Investigation for Paleoenvironment of the Lower Cambrian Niutitang Formation Shales in the Yangtze Platform. *Journal of Petroleum Science and Engineering*, 159: 376 – 386. https://doi. org/10.1016/j. petrol.2017.09.047

Zhu, B., Jiang, S. Y., Yang, J. H., et al., 2014. Rare Earth Element and SRND Isotope Geochemistry of Phosphate Nodules from the Lower Cambrian Niutitang Formation, NW Hunan Province, South China. *Palaeogeography*, *Palaeoclimatology*, *Palaeoecology*, 398: 132 – 143. https://doi.org/10.1016/j.palaeo.2013.10.002

Zhu, M. Y., Zhang, J. M., Steiner, M., et al., 2003. Sinian-Cambrian Stratigraphic Framework for Shallow- to Deep-Water Environments of the Yangtze Platform: An Integrated Approach. *Progress in Natural Science*, 13(12): 951 – 960. https://doi.org/10.1080/10020070312331344710

Zhuang, H. P., Lu, J. L., Fu, J. M., et al., 1998. Organic/Inorganic Occurrence of Metallic Elements of the Black Shale-Hosted Baiguoyuan Silver-Vanadium Deposit in Xingshan, Hubei. *Acta Geologica Sinica*, 72(3): 299 – 307